Composition and provenance of African dust transported over the North Atlantic Ocean

ROEL JAN VAN ZONNEVELD[1]

Supervisors: Dr. Timme Donders[2], Dr. Francesca Sangiorgi[1] and Prof. Dr. Jan-Berend Stuut[3,4]

[1] Faculty of Geosciences, Department of Earth Sciences, Utrecht University, 3584 CB Utrecht, The Netherlands; [2] Faculty of Geosciences, Department of Physical Geography, Utrecht University, 3584 CB Utrecht, The Netherlands; [3] NIOZ, Royal Netherlands Institute for Sea Research, 1790 AB Texel, The Netherlands; [4] Faculty of Science, Department of Earth Sciences, Vrije Universiteit Amsterdam, 1081 HV Amsterdam, The Netherlands

Abstract

(Date of submission: 31-05-2024)

North Africa is considered to be the largest dust producing region of the world, and its transport and deposition have major effects on Earth's climate and environments. Especially the deposition of dust into the Atlantic Ocean has a significant impact on the nutrient distribution, primary production and carbon preservation, which in turn affects our planet on a global scale. While major changes in these trans-Atlantic dust emissions are expected to occur in the near future, the exact effects remain unpredictable due to large information gaps concerning the distribution, source locations and source-to-sink variability of major dust emissions over the Atlantic Ocean. This study therefore presents atmospheric dust samples that are collected across the Atlantic Ocean while sailing from the Canary Islands to Martinique in December 2023. With these samples, the primary objective of this thesis is to identify the main source region for dust transported across the North Atlantic Ocean during boreal winter and to explore downwind changes in its composition. To achieve this, the samples are analysed for grain-size distribution, concentration, bulk chemistry and biological content, and the results are subsequently assessed with the help of satellite imagery, back-trajectory model data and redundancy analyses (RDA). The biological content predominantly consists of freshwater diatoms, especially *Aulacoseira ambigua, Aulacoseira granulata, Epithemia* spp., *Melosira* sp. and *Stephanodiscus* sp., and are interpreted to originate from sedimentary paleolake deposits located near the tri-border area of Algeria, Mali and Niger. Diatoms are abundant until about halfway across the Atlantic Ocean, and some specimens reach as far as the Caribbean. Pollen obtained from the dust samples mainly represent vegetation from the mediterranean, steppe and Sahara regions, while pollen representative for zones south of the Sahara are not present. Overall, high dust concentrations of approximately 0.03 mg m^{-3} day^{-1} are reported and concentrations remained elevated until about two thirds across the Atlantic Ocean. Changes with regards to the grain sizes and bulk chemistry remain minor until about two thirds across the Atlantic Ocean, and changes occur concurrent with the decline in concentration and a reduction in wind speed. Additionally, relatively more monomineral particle fragments are observed for the eastern samples against relatively more clay minerals for the western samples. This relative increase in clay minerals occurs simultaneous with an observed increase in median grain sizes from ~ 3 µm to ~ 4.5 µm, resulting in similar grainsizes between the most western and eastern samples. The majority of the dust samples are interpreted to originate from a major area encompassing northern Mauritania, northern Mali, north-western Niger and southern Algeria. Within this region, a specific dominance is interpreted from paleolakes at the tri-border region of Algeria, Mali and Niger. Only two samples obtained near the Caribbean (A12 - A13) suggest a displacement of the dominant source region within North Africa, while the two most western samples (A14 - A15) potentially originate from the Americas. Finally, since the tri-border region of Algeria, Mali and Niger is currently not recognized as an important source for diatom-rich dust across the Atlantic Ocean, future emphasis is recommended to the role of the paleolakes of this region in providing elevated concentrations of atmospherically dispersed diatoms for trans-Atlantic transport during boreal winter.

Keywords: dust, North Africa, source regions, trans-Atlantic transport, pollen, diatoms

Contents

1. Introduction

In the past years, the atmospheric distribution of dust from the African continent has become increasingly recognized as an important component in many environmental and climatic systems around the world. Especially the Saharan dust deposition into the Atlantic Ocean of approximately 140 Tg each year (Yu et al., 2015) has an enormous influence on this marine environment, even resulting in major climatic effects on a global scale (Prospero & Lamb, 2003; Guo et al., 2012; Moore et al., 2013; Meng et al., 2016). Increased dust fluxes into such marine environments can for example replenish limiting nutrients for primary production, such as P and Fe (Moore et al., 2013), therefore directly stimulating phytoplankton growth and resulting in increased photosynthetically fixed CO_2 (e.g., Prospero & Lamb, 2003; Jickells et al., 2005; Martínez-Garcia et al., 2011). Moreover, major dust input can increase the lithogenic ballasting of organic matter, resulting in enhanced sinking velocities and subsequent increased carbon export and preservation (Klaas & Archer, 2002; Jickells et al., 2005; Pabortsava et al., 2017; Van der Jagt et al., 2018). Since such effects of dust on marine environments are especially important for low-nutrient, low-chlorophyll waters (e.g., Ridame & Guieu, 2002; Moore et al., 2008), the high dust fluxes originating from North Africa have major effects on the oligotrophic regions of the Atlantic Ocean, even to as far as the Caribbean region (Talbot et al., 1986). Another important effect of the African dust fluxes is their major impact on Earth's radiative balance and meteorology. By acting as condensation and ice nuclei, dust can directly alter cloud formation and precipitation processes (Twohy et al., 2009; Karydis et al., 2011; Creamean et al., 2013). Dust distributed at higher altitudes can also result in a direct cooling effect through the obstruction of incoming solar energy, whereas dust distributed at lower altitudes can have the opposite result by trapping energy reflected from Earth's surface (e.g., Claquin et al., 2003; Otto et al., 2007).

While it is therefore clear that African dust distribution has major effects on Earth's climate, projected climatic and environmental changes (IPCC, 2013) are in turn expected to influence future dust emissions (e.g., Pausata et al., 2020). So far, the exact effects on dust emissions remain uncertain due to the complexity of predicting all the combined shifts in natural climate change, anthropogenic climate change and even geoengineering initiatives (Pausata et al., 2020). Nevertheless, changes in African dust emissions are expected to occur with global climate change due to their sensitivity to fluctuations in hydrology and land-use (Pausata et al., 2020). Therefore, due to the impact of dust emissions on the marine environment and Earth's radiative balance, the study of African dust transport and deposition is of increasing importance.

Studying dust accumulations in marine sediments also assists in the interpretation of paleo-environmental and paleo-climatological changes (Tiedemann et al., 1994; Grousset et al., 1998; Cole et al., 2009). This is particularly relevant for the northern part of the African continent, since distribution of land-derived sediments in this region is primarily governed by eolian transport processes (Demenocal et al., 2000; Moreno et al., 2001). Research by Stuut et al. (2005) indicates a clear similarity between aerosol samples taken above the tropical North Atlantic Ocean and the lithogenic fraction on its seafloor. Therefore, information on the biological content (e.g. pollen), transportation and origin of modern mineral dust will help in the climatic and environmental interpretation of geological archives.

Unfortunately, there are large gaps in our knowledge concerning the trans-Atlantic distribution of significant dust emissions and the source-to-sink variability of emitted dust. This lack of information affects the baseline from which to monitor change in dust emissions and the resulting environmental and climatic impact. Moreover, different studies on specific dust sources for this trans-Atlantic transport provide contradictory results (e.g., Herrman et al., 1999; Scheuvens et al., 2013; Jewell et al., 2021), resulting in multiple different geographical descriptions of the North African source areas. This restrains further understanding of source-to-sink relations, and hence, complicates studies on dust-climate relations and paleoclimatic studies using dust archives. This overall deficiency of information on

African dust and its distribution over the Atlantic Ocean is mainly attributed to the fact that most of the information is either restricted to areas on the continental shelf or primarily derived from marine sediments instead of the atmospheric particles themselves (Stuut et al., 2005). More information on dominant source locations and downwind distributional characteristics is therefore needed.

In this thesis, a set of dust samples is presented that were collected over the Atlantic Ocean while sailing from the Canary Islands to Martinique aboard the clipper Stad Amsterdam in December 2023. This data set provides the unique opportunity to study downwind changes in North African dust emissions during boreal winter, with emphasis on composition and origin. With these samples, the aim of this thesis is to identify the main source locations for dust transport across the North Atlantic Ocean during boreal winter, as well as to quantify variations in quantity and composition along this transect. To achieve this, the samples are analysed for their physical and chemical properties as well as the biological content. The results are subsequently compared to satellite imagery, back-trajectory model data and results from redundancy analyses to interpret changes in the obtained dataset.

2. Background on transport characteristics and regional setting

2.1. Transport characteristics

Previous studies on African dust distribution have identified several selective transport characteristics along the downwind trajectory of dust emissions. Firstly, dust plumes have an overall well-sorted distribution, and grain sizes along the African coast usually lie between 8 μm and 42 μm (Stuut et al., 2005). There are however frequent exceptions of sizes up to 200 μm along the coast (Stuut et al., 2005), as well as reports of long-range transport of particles larger than 75 μm (e.g., Van Der Does et al., 2018). During boreal winter, sorting is more pronounced and grain sizes are generally smaller when compared to boreal summer (Friese et al., 2016). Mean grain sizes along the downwind trajectory across the Atlantic Ocean generally show a decrease from ~90 μm at the Cape Verde Islands to ~5 μm near the Caribbean, which is attributed to a higher settling velocity for larger particles (Glaccum & Propero, 1980; Talbot et al., 1986). In general, such changes in grain-size distribution become relatively small after transportation of about 1000 km (Reid et al., 2008). Additionally, monomineral particle fragments, which mainly originate from the large sand seas of North Africa, have a wider size distribution when compared to clay mineral aggregates, which mainly originate from the borders of the Sahel (Stuut et al., 2009). In general, particles larger than ~2 μm mainly consist of primary minerals produced during rock formation, such as quartz, plagioclase, K-feldspar, amphibole, biotite and muscovite (Glaccum & Prospero, 1980; Knippertz & Stuut, 2014), while particles of ~2 μm or smaller mainly consist of clay minerals such as mica, kaolinite, smectite, vermiculite, chlorite, palygorskite and sepiolite (Glaccum & Prospero, 1980; Knippertz & Stuut, 2014). Due to a relatively larger grain size and settling velocity, a decrease in concentration of quartz, plagioclase, microcline, and calcite is expected windwards against an increase in clay minerals (Glaccum & Prospero, 1980). Finally, a difference in dominant wind systems between summer and winter period (see section 2.2.) causes coarser dust particles to remain in suspension for longer time periods during boreal summer. This results in overall larger grain sizes observed further from the continents compared to boreal winter (Korte et al., 2016; Van Der Does et al., 2016; Korte et al., 2017).

2.2. Wind systems

There are two main wind systems in northwestern Africa that transport large quantities of dust during the winter period; the northeastern trade winds and the Harmattan winds (Figure 1; Figure 2). The northeastern trades are considered as one of the most important wind systems for dust transport, are active year-round and reach as far as the ITCZ (~5° S in winter) (Nicholson, 2000; Stuut et al., 2005; Hooghiemstra et al., 2006; Adams et al., 2012; Van Der

Does et al., 2016). It transports large quantities of considerably dry dust and is active between the surface to about 1000 m altitude (e.g., Hooghiemstra et al., 2006). With these trade winds, Saharan dust is transported parallel to the coast from the Atlas Mountains across the Sahara towards the eastern Atlantic Ocean (Pye, 1987). The northeastern trade winds do not carry the dust very far and usually deposit it between the coast and the Canary and Cape Verde Islands (Pye, 1987; and references therein).

The Harmattan winds are officially part of the northeastern trade winds and are active in the southern regions of North Africa (Prospero & lamb, 2003; Tsamalis et al., 2013). These winds are particularly active during boreal winter and are an important transport system for dust at altitudes between 0 and 3 km (McTainsh, 1980; Prospero & lamb, 2003; Tsamalis et al., 2013). Especially during winter, the cold and dry Harmattan winds transport large amounts of nutrient-rich dust southwards across the Atlantic Ocean (Prospero & Lamb. 2003).

Another wind system in northwestern Africa that plays a major role in dust distribution across the Atlantic Ocean is the African Easterly Jet (AEJ) and typically operates between 3000 and 5000 m altitude (Pye, 1987; Adams et al., 2012; Tsamalis et al., 2013). The AEJ is an active wind system and causes maximum wind speeds within the dust-laden air mass of the Saharan Air Layer (SAL), which is a deep mixed layer of hot and dry air that is characteristic for long-range dust transport (Nicholson, 2013; Tsamalis et al., 2013). Both the AEJ and SAL are mainly dominant during boreal summer and play a major role in the long-range dust transport from Africa to the Americas (Pye, 1987; Stuut et al., 2005; Tsamalis et al., 2013). During boreal winter however, the AEJ is being replaced by a dominant westerly wind known as the anti-trades (e.g., Hamilton et al., 1945; Nicholson, 2000). Therefore, since much of the dust deposited far away is transported by the AEJ, lower concentrations are deposited in the western part of the Atlantic Ocean during the winter period (Adams et al., 2012; Tsamalis et al., 2013; Van Der Does et al., 2016).

2.3. Source regions

While North Africa is known for its vast sand seas, most of the region is actually not that important when it comes to dust production (Goudie & Middleton, 2001; Prospero et al., 2002; Engelstaedter et al., 2006; Schepanski et al., 2009; Scheuvens et al., 2013). This is mainly due to the overall large grain sizes in these sand seas, preventing the sediments to gain enough altitude to be transported over longer distances (Scheuvens et al., 2013). There are however multiple regions within North Africa that contain grain sizes small enough for major dust production. Jewell et al. (2021) defined these areas and presented three major potential dust sources (SA1 - SA3) by combining their own data with geographically defined source regions from previous studies (mainly from Schepanski et al. (2012) and Scheuvens et al. (2013)). A general description for each of these regions is provided below and a visual representation is given in Figure 1.

The first source area (SA1) is described by Jewell et al. (2021) to be the area encompassing northern Mauritania, northern Mali, north-western Niger, and southern Algeria. The area is enclosed by the Atlantic Ocean to the west, the Atlas Mountains to the north and the Hoggar (southern Algeria) and Aïr (northern Niger) Mountains to the east, separating this region from the second source area (SA2). Much of the dust in this region is picked up by the northeastern trades and plays an important role in dust transport across the North Atlantic Ocean. Dust production in this source area is mainly dominated by alluvial deposits and multiple smaller paleolakes of Pliocene and Pleistocene age located below the Hoggar Mountains near the tri-border region of Algeria, Mali and Niger (Gasse et al., 1989; Scheuvens et al., 2013; Evan et al., 2015; Jewell et al., 2021). The second source area (SA2) is situated on the borders of Chad and Niger and is enclosed by the Tibesti and Ennedi Mountains to the north. Dust production in this source

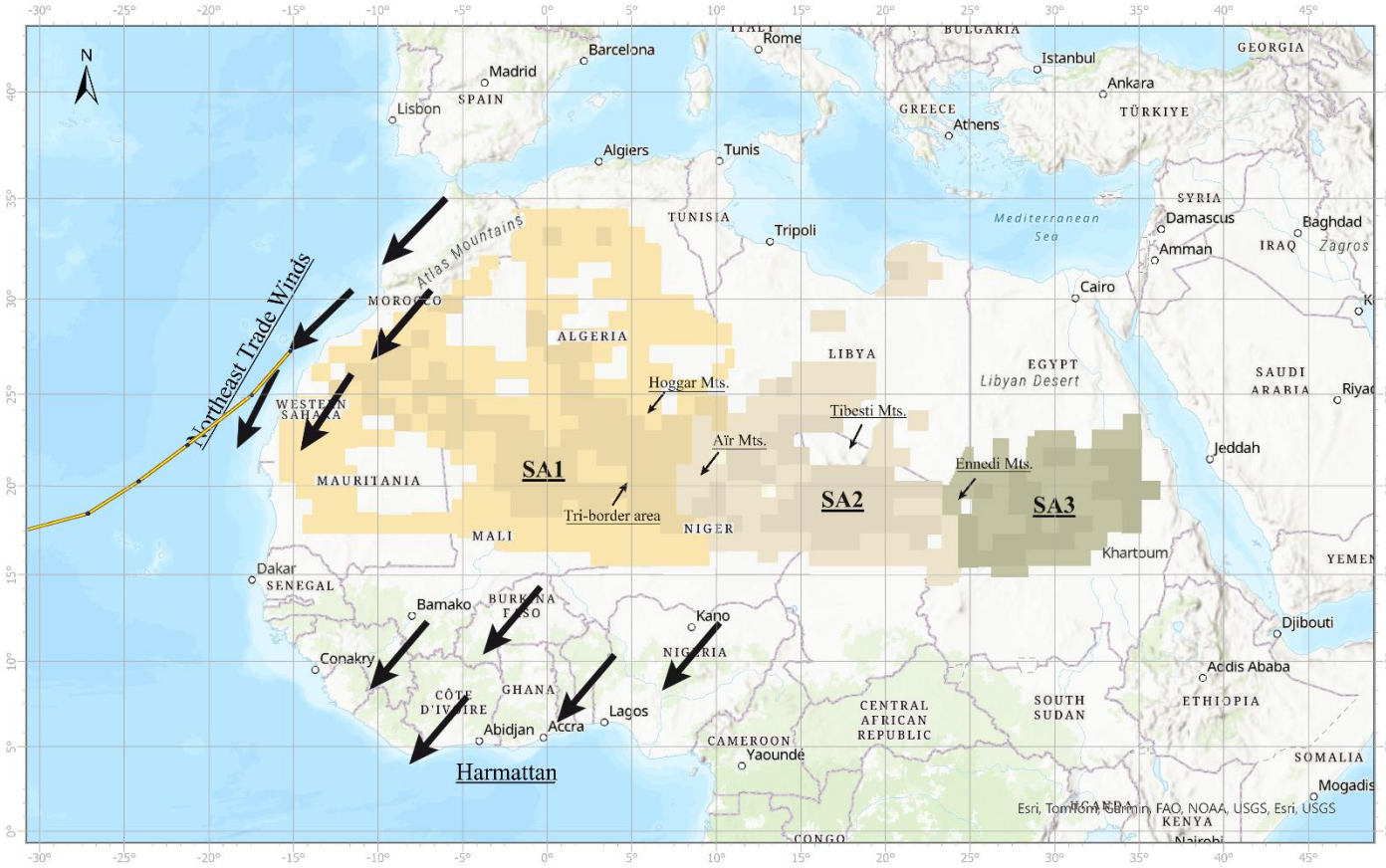

Figure 1: *Map of northern Africa showing major potential dust sources (SA1 – SA3), with darker colours representing regions with more active dust production (modified after Jewell et al. (2021)). Additionally, the two most relevant wind systems for dust transport during boreal winter and part of the sampling route used for this study are provided.*

area is dominated by the sedimentary deposits from the Bodélé Depression and paleoriver systems such as the Bahr El Gazel, which are located within the areal extent of paleolake Megachad (Bristow et al., 2009; Lécuyer et al., 2016; Jewell et al., 2021). Both the Bodélé depression and the paleoriver systems contain significant diatomite deposits of Holocene and Pleistocene age (Servant, 1983), and disperse large numbers of diatoms through the Harmattan winds to regions as far as South America (e.g., Kalu, 1979; Gasse et al., 1989 and references therein). Dust transport from this region is intensified through the Tibesti and Ennedi Mountains, which funnel strong near surface winds coming from the northeast. These strong surface winds combined with the low density of diatom-rich sediments make this region by far the largest and most active dust source in Africa (Bristow et al., 2009; Washington et al., 2006) and is estimated to produce up to 64% of the North African dust emissions (Evan et al., 2015). Finally, the Eastern source region is enclosed by the Ennedi Mountains to the West and the Red Sea to the East and dust production in this region is mainly dominated by alluvial deposits within the Nubian Desert of Sudan (Bakker et al., 2019).

Of these three source regions, SA1 and SA2 are considered most important for transport to the Atlantic Ocean (Scheuvens et al., 2013), with SA1 being distinctly active during boreal summer and SA2 being active year-round (Schepanski et al., 2007; Ben-Ami et al., 2012). Moreover, Moreno et al. (2006) suggest the possibility of mixing of these different source regions, to then commonly move westwards across the Atlantic Ocean and eventually converge with dust from the northwestern coast above the Atlantic Ocean between 10°N and 25°N. Nonetheless, contradictory results continue to persist and information concerning dust transport, composition and influence of these source regions remains insufficient as a result of political or geographical complications (Knippertz & Stuut, 2014). More information on these source regions and their influence is therefore definitely required.

2.4. Chemical signals

Many regions in North Africa have distinct chemical properties and an overview of the chemical compositions of regions considered relevant to this study is provided in this section. The most northern part of Africa (but also Western Sahara and the Canary Islands) is known for a low aluminium content and is characterised by a noticeably higher phosphorus content (Rodríguez et al., 2011; Scheuvens et al., 2013). The high phosphorus content is most likely the result of a few phosphate deposits, mines and biomass burning in the northern regions (Rodríguez et al., 2011). The region encompassing western Mauritania and Western Sahara has rather high calcium and magnesium contents, while the region at the tri-border area of Algeria, Mali and Niger displays an overall heterogeneous chemical composition (Scheuvens et al., 2013). This heterogeneous composition is the result of the large amount of small sedimentary paleolake deposits, with each paleolake having its own distinctive sedimentary composition. Nevertheless, rather high values of aluminium were reported for the northern part of this region, close to the Hoggar Mountains (Scheuvens et al., 2013 and references therein). The Bodélé depression in SA2 is known for its unusually high silica values, high titanium values and slightly higher phosphorus values (Mounkaila, 2006; Bristow et al., 2010). The region is however most distinguishable by its compositional inhomogeneities in its calcium contents and quite low values for (Ca+Mg)/Fe ratios (Bristow et al., 2010; Scheuvens et al., 2013).

Especially the distinct regional signals for calcium and magnesium prove effective in distinguishing different dust sources across North Africa (Scheuvens et al., 2013). Mainly by using ratios of (Ca+Mg)/Al or (Ca+Mg)/Fe, a distinction between the potential dust sources can become visible (Scheuvens et al., 2013). However, some studies have indicated that smaller local areas within the major source areas are rather heterogeneous in composition (e.g., Mounkaila, 2006), which therefore possibly affects the signal. Nevertheless, Scheuvens et al. (2013) suggest that the mixing of these smaller areas together with a persistent 'regional background aerosol signal', will result in dust signals that are quite homogeneous in composition when viewed on a regional scale. This is also clearly substantiated by their compiled data set and various regions are therefore considered to provide distinct "fingerprint" signals that can be used to make a connection between atmospheric dust samples and potential source areas in North Africa.

2.5. Vegetation zones and biological markers

In addition to the chemical composition, biological remains within dust plumes can also provide data on distinct source regions. Darwin had already realised this during his voyages aboard the HMS Beagle, during which multiple phytoliths (microscopic silica structures from plant cells) and "silicious-shielded protozoans" with a freshwater origin were detected (Darwin, 1846). Beside these siliceous remains, pollen assemblages derived from dust plumes can also provide data on dust sources and transportation mechanisms. Pollen data derived from dust traces within marine sediments is therefore frequently used for paleo-environmental and paleo-climatic studies of North Africa (e.g., Tiedemann et al., 1994; Grousset et al., 1998; Cole et al., 2009). Moreover, since the majority of the pollen in the surface atmosphere are freshly emitted and so, provide an accurate representation for corresponding vegetation areas (Calleja et al., 1993; Hooghiemstra et al., 2006), pollen data from modern dust samples can also act as an additional verification in order to retrace dust to its original source.

The distribution patterns of pollen within dust plumes are generally different compared to the inorganic fraction (Hooghiemstra et al., 2006). This is because different pollen species resemble different distribution patterns, for example through the use, or disuse, of air-filled bladders (Schwendemann et al., 2007). An overview of these distribution patterns is provided in the isopollen maps from Hooghiemstra et al. (2006). Nonetheless, these isopollen maps are based on data from marine surface sediments and only few studies have actually investigated palynological data derived from air samples (e.g., Melia, 1984). The isopollen maps therefore form a basis in understanding modern

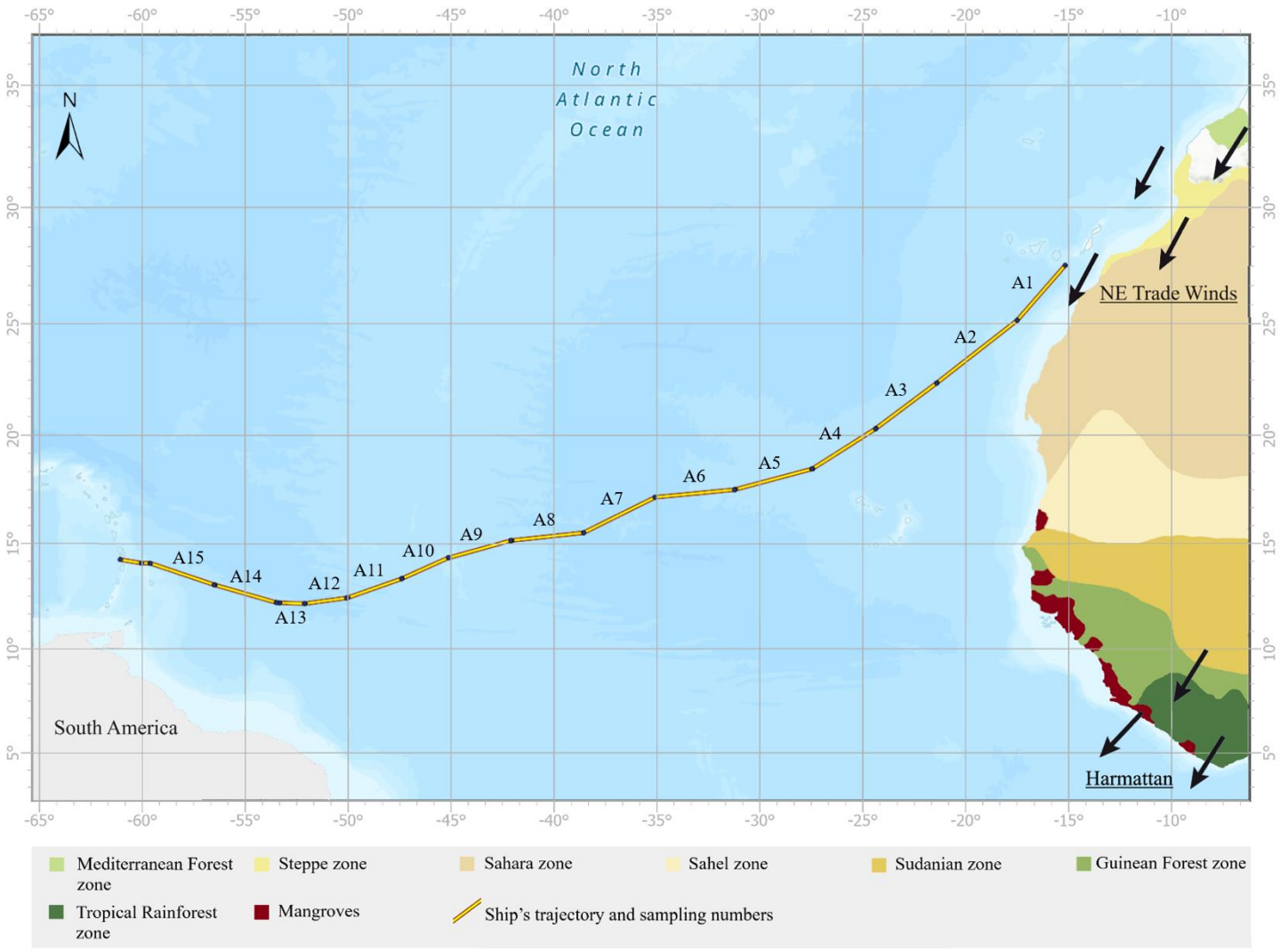

Figure 2: *Map showing modern vegetation zones in northwestern Africa (modified after Hooghiemstra et al. (2006)), an overview of the ship's trajectory and sampling locations, and the two most relevant wind systems for dust transport during boreal winter.*

pollen distribution from Africa across the Atlantic Ocean, and can be compared to observations made in the actual aerosol data provided in this study.

The distribution of various pollen species across the Atlantic Ocean is mainly coupled to North Africa's vegetation zones, which are conveniently characterised from north-south (White, 1983). Due to the well-defined differences in vegetation for each of these zones, pollen assemblages found off the west coast of Africa can be linked to corresponding vegetation zones (Gajewski et al., 2002). An overview of these vegetation zones is given in Figure 2 and a short description on their pollen assemblage is provided below.

The most northern zone is covered by mediterranean forests and is therefore mainly dominated by *Quercus*, as well as *Alnus*, *Pinus*, *Olea* and *Betula* (Dupont, 1999; Hooghiemstra et al., 2006). To the south of this belt lies the Steppe zone, which is dominated by *Artemisia* and in part indicated by Chenopodiaceae-Amaranthaceae and E*phedra* (Dupont, 1999; Hooghiemstra et al., 2006). Chenopodiaceae-Amaranthaceae and *Ephedra* are however mainly dominant in the desert vegetation of the subsequent Sahara zone (Dupont, 1999; Gajewski et al., 2002; Hooghiemstra et al., 2006). While Poaceae and Cyperaceae are both widely distributed and abundant in most vegetation zones (Gajewski et al., 2002; Hooghiemstra et al., 2006), Poaceae pollen are especially dominant in the Sahel zone which results in typical savannah vegetation (Dupont, 1999; Hooghiemstra et al., 2006). In the Sudanian zone, the

woodlands return and the genera *Combretum* and *Mitracarpus* become clear markers for this section (Hooghiemstra et al., 2006). The last two zones to the south, the Guinean Forest zone and the Tropical Rainforest zone, have a highly diverse floral composition and plants are mainly pollinated by insects (Gajewski et al., 2002). A typical wind-dispersed pollen signal with certain dominant genera is therefore not expected for these zones (Gajewski et al., 2002). In addition to these zones, loose patches of mangrove bands that are characterised by *Rhizophora* can be identified, as well as one region with *Avicennia* mangroves (Hooghiemstra et al., 2006). Even though the Canary Islands are not categorised as a distinctive zone, *Pinus* is typical for these islands and is certainly displayed in the pollen signal across this part of the Atlantic Ocean (Hooghiemstra et al., 2006).

3. Methods

Samples for this project are collected during an ocean crossing from the Canary Islands (Las Palmas de Gran Canaria) to Martinique (Fort-de-France) and took place from December 13th until December 28th. The exact sampling locations are provided in Table 1 and a visual overview of the ship's trajectory and sampling locations is given in Figure 2 and Figure 4a. Daily measurements of wind speed, wind direction, air temperature and air pressure (Table 2) are derived using equipment available on the bridge of the ship and coordinates are obtained using the ship's own navigation system.

Samples are collected aboard the sailing vessel Stad Amsterdam, which, due to the overall lack of engine use, provided the proper conditions to conduct aerosol sampling. It must be noted however that, due to the absence of wind during the last part of the trajectory, the engine was turned on between 12°19.250 N - 53°07.418 W and 14°10.952 N - 60°08.156 W, providing the possibility of minor disturbance for samples A13 - A15. A visual alteration as a result of the ships exhaust gasses is only observed for sample A13, which expressed itself in a dark-grey colouring of the filter. The dark-grey colour of sample A13 disappeared after filtering and the disturbance does not show any distinct alterations in the results.

Air samples are collected using a dust sampler from the Royal Netherlands Institute for Sea Research (NIOZ). This sampler consists of a metal housing (~ 40 x 40 x 130 cm) containing a vacuum-cleaner engine and was positioned at ~8 m above sea level (asl). Approximately 1.14 m^3 air was sucked through a cellulose filter (20.3 x 25.4 cm) every minute, with an average exposure time of about 23.5 hours for each sample. One quarter of each filter is used to analyse the organic content while another quarter is used to analyse the mineralogical characteristics. The remaining two quarters are stored in case of data loss and possible future use.

Microscope slides for biological analyses are prepared in the GeoLab at Utrecht University. Dust is rinsed off the filters using a basic spray bottle and water before being sieved through a 10 µm sieve. The samples are held in an ultrasonic bath for approximately one minute, centrifuged for 5 minutes at 2200 rpm (acceleration setting 9, deceleration setting 0) and subsequently transferred into Eppendorf Safe-Lock Tubes. Finally, after another 5 minutes in the centrifuge, the samples are mounted on microscope slides using Glycerine Jelly and embedded with Paraplast. The resulting slides are analysed using an Olympus CX21 Phase Microscope and photographed using a Leica MC170 HD standalone microscope camera mounted on a Leica DM2500 LED Optical Microscope. Taxonomic information used for algae identification is retrieved from the content curation community at diatom.org and algaebase.org (Guiry & Guiry, 2020; Spaulding et al., 2021). Pollen identification is carried out using the pollen atlases provided by Reille (1999) and Gosling et al. (2013). Finally, it must be noted that the quantitative results of the biological fraction should be considered with caution due to the possibility of material being left behind on the filter.

Sample number	Date		Position (lat. N)	Position (long. E)	Total duration (min.)	Total flow (m^3)
A1	13/12/2023	Start	27°53.366	−15°16.860	1326.3	1506.38
	14/12/2023	Stop	25°14.228	−17°51.142		
A2	14/12/2023	Start	25°14.171	−17°51.271	1484.9	1686.26
	15/12/2023	Stop	22°37.940	−21°39.628		
A3	15/12/2023	Start	22°36.424	−21°42.158	1424.1	1617.17
	16/12/2023	Stop	20°32.416	−24.35.897		
A4	16/12/2023	Start	20°30.82	−24°38.104	1416.2	1607.80
	17/12/2023	Stop	18°47.930	−27°44.528		
A5	17/12/2023	Start	18°47.032	−27°46.974	1420.1	1612.72
	18/12/2023	Stop	17°52.517	−31°19.946		
A6	18/12/2023	Start	17°51.575	−31°23.426	1492.2	1694.78
	19/12/2023	Stop	17°16.661	−35°08.720		
A7	19/12/2023	Start	-17°15.521	-−35°11.513	1404.2	1595.01
	20/12/2023	Stop	15°54.317	−38°49.308		
A8	20/12/2023	Start	15°51.903	−38°55.997	1401.8	1592.15
	21/12/2023	Stop	15°15.750	−42°06.799		
A9	21/12/2023	Start	15°15.297	−42°09.529	1422.9	1616.54
	22/12/2023	Stop	14°35.036	−45°09.881		
A10	22/12/2023	Start	14°35.170	−45°12.020	1476.3	1676.74
	23/12/2023	Stop	13°37.140	−47°37.588		
A11	23/12/2023	Start	13°36.386	−47°38.721	1437.4	1632.56
	24/12/2023	Stop	12°46.927	−50°00.919		
A12	24/12/2023	Start	12°46.065	−50°05.347	1405.7	1596.42
	25/12/2023	Stop	12°18.992	−52°08.631		
A13	25/12/2023	Start	12°19.015	−52°10.494	1306.2	1483.30
	26/12/2023	Stop	12°22.691	−53°32.469		
A14	26/12/2023	Start	12°24.140	−53°48.810	1417.0	1609.87
	27/12/2023	Stop	13°06.851	−56°46.070		
A15	27/12/2023	Start	13°07.909	−56°49.986	1407.0	1597.81
	28/12/2023	Stop	14°09.108	−59°59.708		

Table 1: *Overview of sampling positions, total sampling time and total flow of all air samples (N = 15).*

Grain-size analyses and bulk chemical analyses are performed in the laboratory of NIOZ. For the grain-size analyses, filters are ashed for 48 hours using a Low Temperature Asher (Tracer Lab, Model LTA 600) after which the samples are transferred into ~200 ml of de-gassed R/O water. Particle sizes are then measured with a Coulter laser particle sizer (LS 13 320) using a universal liquid module for samples A1 - A13. A micro liquid module is used for samples A14 - A15 due to an insufficient amount of dust for the universal liquid module. No reagents are used for chemical dispersion in order to prevent particles from sticking together. Instead, a magnetic stirrer present in the particle sizer

Date	Sample numbers		Air temperature (°C)	Air pressure (mb)	Absolute wind direction (degr.)	Absolute wind speed (m/s)
	Stop	Start				
13/12/2023		A1	23.9	1017	065-075	4.4
14/12/2023	A1	A2	25.7	1017	080-090	13.9
15/12/2023	A2	A3	25.5	1017	070-080	9.8
16/12/2023	A3	A4	25.9	1014	060-080	11.1
17/12/2023	A4	A5	27.7	1013	070-080	9.5
18/12/2023	A5	A6	27.8	1013	075-085	7.5
19/12/2023	A6	A7	28.2	1016	070-090	7.7
20/12/2023	A7	A8	29.4	1013	080-100	9.3
21/12/2023	A8	A9	30.8	1013	090-100	8.5
22/12/2023	A9	A10	30.4	1015	070-100	6.9
23/12/2023	A10	A11	31.1	1014	050-080	5.1
24/12/2023	A11	A12	31.5	1011	070-100	6.2
25/12/2023	A12	A13	31.7	1013	070-95	4.9
26/12/2023	A13	A14	33.5	1013	50-120	2.8
27/12/2023	A14	A15	31.5	1013	130-150	3.7
28/12/2023	A15		29.7	1013	035-45	2.6

Table 2: *Daily measurements of wind speed, average margins of wind direction, air temperature and air pressure. Measurements are obtained between the end of one sample and the beginning of another (approximately around 12:30 h local time).*

is used to homogenise the dust samples. After grain-size analysis, the dust samples are transferred onto pre-weighed circular filters of 25 mm Ø (nuclepore track-etch membrane filters, 0.2 µm) and weighed again on a micro-balance to obtain total dust mass, and so, the total concentration. Finally, the samples are freeze dried and analysed for the elemental composition by X-ray fluorescence (XRF) using the Avaatech XRF core scanner (Richter et al., 2006). All measurements are conducted 5 times and average values of these measurements are used in analysing the data.

Back-trajectories are calculated using the Hybrid Single-Particle Lagrangian Integrated Trajectory (HYSPLIT) model of the National Oceanic and Atmospheric Administration (NOAA) (Stein et al., 2015; Rolph et al., 2017). By using HYSLPLIT on the READY system available on the NOAA's website, 5-day back-trajectories are calculated beginning from the altitude at which the samples have been collected (~8 m), as well as from 500 m and 5000 m altitude. In addition to the HYSPLIT model, true colour satellite images are used to aid in the interpretation of downwind variations in grain size, concentration, biological aerosols and bulk chemical characteristics. Images are downloaded using the NASA Worldview application (https://worldview.earthdata.nasa.gov) which is part of the NASA Earth Observing System Data and Information System (EOSDIS). Finally, the relationship between independent variables and multiple explanatory variables are examined using redundancy analyses (RDA) with the aid of the PAST software package available at https://www.nhm.uio.no/english/research/resources/past/ (Hammer & Harper, 2001).

During fieldwork, daily water samples are collected in addition to the air samples. Each day about 40 L of water is collected from the ocean's surface using a bucket and sieved through a 10 µm sieve, concentrating the water samples into sampling bottles of 100 ml. About three drops of neutrally buffered formaldehyde solution (~4%) is added to the water samples with the aim of preserving the material. Unfortunately, this proved unsuccessful for some samples which showed abundant microbial activity after review in the laboratory. This, in combination with time constraints, resulted in the decision to refrain from using the water samples for this thesis. The water samples are stored in the Earth Simulation Laboratory at the University of Utrecht for possible further use. An overview of the sampling locations and properties of the water samples is provided in Table S1.

4. Results

High dust concentrations of approximately 0.03 mg m^{-3} day^{-1} are reported for the initial two thirds of the sampling route, after which the concentration decreases gradually from east to west to approximately 0.002 mg m^{-3} day^{-1} for the most western samples (Figure 4b). Beside this general trend, significant lower concentrations of about 0.015 mg m^{-3} day^{-1} can be observed for samples A2 and A3, after which the concentration increases again to previous levels. The absolute abundance of both pollen and algae in the air samples shows a rather similar trend (Figure 4c), however with a few distinct differences. Distinct lower levels in the absolute abundance of pollen and algae can be observed for samples A2 and A3, but, in contrast to the concentration, also for sample A4 (Figure 4c). The numbers of pollen and diatoms increase again to previous levels at sample A5, after which a gradual decrease occurs until about two thirds across the Atlantic Ocean. Diatoms and pollen remain the dominant biological components in the dust until about halfway of the sampling route, after which fungi spores become relatively dominant and remain so until the end of the sampling route (Figure 4d).

The bulk grain-size distributions and an overview of changes in the median grain size are given in Figure 5. The results from the grain-size analysis for samples A14 - A15 demonstrate unrealistically high results in comparison with the other samples (median grain size A14 = 50.5 µm; median grain size A15 = 38.5 µm). The reason why grain-size analysis of samples A14 - A15 shows such unrealistic results remains unclear and these samples are therefore

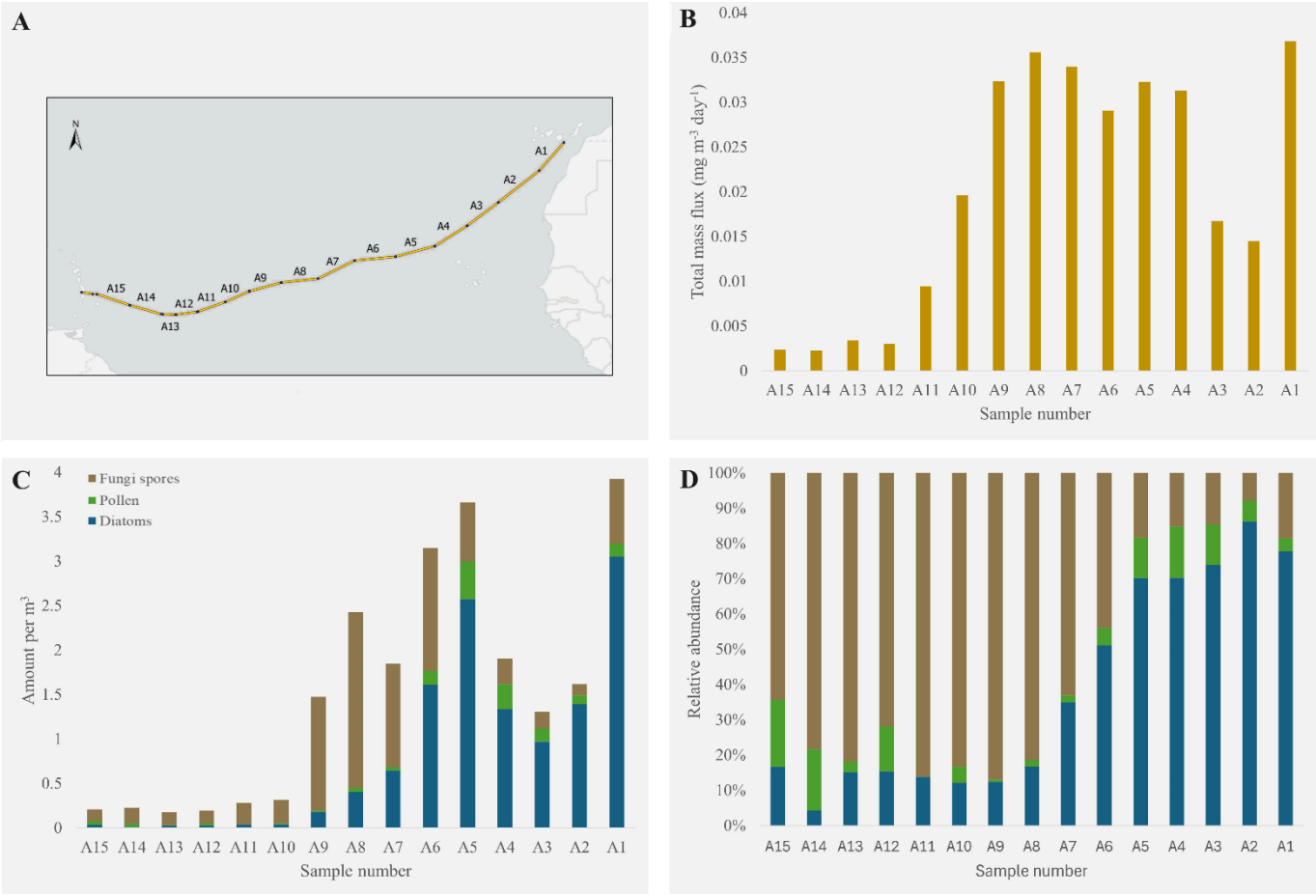

***Figure 4: (A)**: Schematic overview of sampling route and sampling numbers; **(B)**: Concentration of dust in each air sample (mg m^{-3} day^{-1}); **(C)**: Column chart depicting the absolute abundance of algae, pollen and fungi spores found in the air samples (amount per m^3), as well as a legend for graphs C and D; **(D)**: Column chart depicting the relative abundance of algae, pollen and fungi spores found in the air samples (%).*

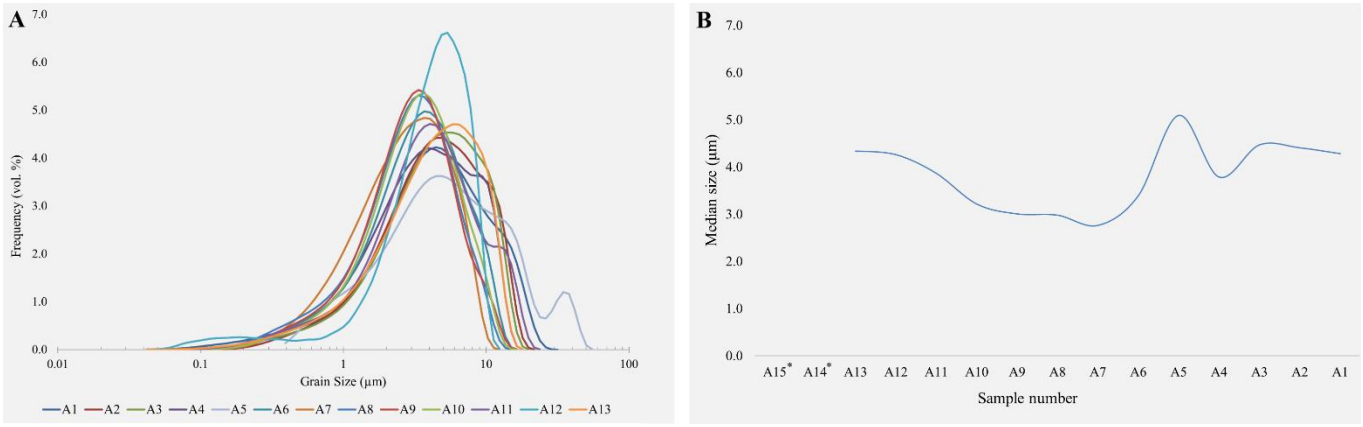

Figure 5: *Grain-size measurements of dust samples A1 - A13. * Samples A14 and A15 are disregarded due to unrealistic results* ***(A)****: Grain-size distribution;* ***(B)****: Median grain size.*

disregarded in this study. In contrast, grain-size analysis of the other samples demonstrate more realistic and reliable results. The median grain sizes (Figure 5b) lie between 4.3 - 5.1 µm to about a third of the sampling route (sample A5), with only a minor drop to 3.8 µm for sample A4. Subsequently, a gradual downwind decline to about halfway across the Atlantic Ocean (sample A7) is observed, resulting in median grain sizes of ~ 3 µm for the successive samples. Changes in median grain size remain minimal to about two thirds of the sampling route (sample A10), after which grain sizes gradually increase to a median size comparable to the eastern samples off the coast of Africa (~ 4.3 µm). Additionally, the grain-size distribution shown in Figure 5a appears to be overall well-sorted and unimodal. Moreover, samples A6 - A11 have sharp peaks between 2 µm and 6 µm, while samples A1 - A4 and A12 - A13 have slightly wider peaks between 4 µm and 10 µm. The distribution for samples A4, A5 and A11 stands out due to a small coarse shoulder at ~ 11 µm (A4), ~ 36 µm (A5) and ~ 13 µm (A11).

Results from the XRF-analysis are visualised for the ratios of Si/Al, (Ca+Mg)/Fe, Fe/Al, Ca/Al and Fe/Si (Figure 6) and an overview of the absolute counts for each separate element is provided in the supplementary materials (Tables S2 - S3). Log-ratios are used to the interpret relative concentrations of certain elements in order to minimize the risk of incorrect interpretations as a result of downwind changes in physical properties (Weltje & Tjallingii, 2008). Some values of the absolute counts are considered invalid due to irregularities with regards to the standard deviation and are therefore not included in the figures or supplementary materials. Absolute counts are measured with both 10 Kv and 30 Kv, depending on the element, and the presented figures are constructed using only the results from 10 Kv.

The absolute numbers of algae, pollen, spores, phytoliths and trichomes (fine outgrows found on the exterior of plants, algae and other protists) observed in the air samples are given in Tables 3 and 4. Images of selected examples of these biological particles are provided in Plates S-I to S-VI. Cellular content remained present in these samples, which occasionally complicated identification. A few findings remain therefore unidentified (Tables 3 and 4; Plates S-II and S-VI), but are reported in the interest of providing a full account and an overview in absolute numbers. Only one trichome has been found and, due to its considerable size (Plate S-III, 8-9), most likely originates from a plant. Some *Aulacoseira* spp., and one cf. *Phacotus* sp. (sample A4) contain what looks like cellular content, of which examples are depicted in Plate S-1 (5-7) and Plate S-II (12-13). Both algae and pollen have at least been identified at the family level and, if possible, at genus level. Some diatoms, such as *Eunotia pierrefuseyi* (Plate S-I, 14-16) and multiple species for *Aulacoseira* (Plate S-I, 1-12), have been identified at the species level due to clear dissimilarities, outstanding preservation and, for some, a potential significance which will be considered in the discussion section.

Sample numbers →		A15	A14	A13	A12	A11	A10	A9	A8	A7	A6	A5	A4	A3*	A2*	A1	Plate
Family	**Genus / species**																
Diatoms																	
Aulacoseiraceae	*Aulacoseira granulata*	1		1		2	2	12	10	13	29	58	48	47½	61	133	S-I
Aulacoseiraceae	*Aulacoseira ambigua*	6	2	4	4	3	5	22	62	100	267	378	186	96	164 ½	312	S-I
Aulacoseiraceae	*Aulacoseira granulata var. angustissima*				1	2	3	2		1		1					S-I
Aulacoseira containing cellular content		0	1	0	1	0	0	0	3	5	15	37	10	38	88	89	S-I
Bacillariaceae	*Nitzschia*														½	1	S-I
Eunotiaceae	*Eunotia pierrefuseyi*							1					1				S-I
Fragilariaceae	*Fragilaria*										8						S-I
Melosiraceae	*Melosira*							1		1	1	4	6	½	1½		S-I
Rhopalodiaceae	*Epithemia* spp.											4	2	½		2	S-I
Rhopalodiaceae	*Epithemia gibba*											4		½	1	2	S-I
Stephanodiscaceae	*Stephanodiscus*							1	3	2	4	18	12	9	4	18	S-II
Stephanodiscaeae	*Cyclotella*					1											S-II
Large unidentified diatom 1																1	S-II
Chlorophytes																	
Phacotaceae	cf. *Phacotus*				1	1			2	1	1	1	3				S-II

Table 3: *Amount and type of algae found in approximately ⅛ filter for each air sample. * ~ ¼ filter is used for samples A2 and A3, which are therefore corrected to amounts comparable to ~ ⅛ filter. Absolute numbers per m^3 are calculated and presented in Figure 4C.*

Sample collection coincided with multiple major dust outbreaks and both the results from the 5-day back trajectories (Figure 7) and the satellite images (Figure 8) show the pathway of these major dust plumes to lead back to northwestern Africa, while higher wind currents trace back towards the American continents (Figure 7c). Visual presence of dust plumes over the sampling route can be interpreted using the satellite images in Figure 8, if keeping in mind that the images only provide snapshots of the first few hours of the sampling route. These satellite images then reveal major dust plumes to almost completely cover the sampling route for samples A1, A2, A5, A6, A7 and A10, partially cover the sampling route for samples A3, A9 and A11 and barely or not cover the sampling route for samples A4, A8, A12, A13, A14 and A15.

Sample numbers →		A15	A14	A13	A12	A11	A10	A9	A8	A7	A6	A5	A4	A3*	A2*	A1	Plate
Family	**Genus**																
Pollen and spores																	
Amaranthaceae-Chenopodiaceae	spp.								2			1	1	1½		3	S-IV
Asteraceae	*Artemisia*		1	1	1				4	3	3	7	3	4	4	3	S-IV
Betulaceae	*Alnus*	2	1				1		1								S-IV
Betulaceae	*Corylus*													1			S-IV
Brassicaceae	cf. *Neslia*										1	2	2	1	1		S-IV
Campanulaceae	*Campanula*		1				1										S-IV
Cannabaceae	*Cannabis*		1														S-IV
Cyperaceae	spp.							1		3	23	47	28	12½	7½	2	S-IV
Ephedraceae	*Ephedra* spp.						1					2					S-IV
Fabaceae	*Acacia*														½		S-V
Liliaceae	*Ornithogalum*									1	1						S-V
Lamiaceae	Sp.				1												S-V
Oleaceae	*Ligustrum*											1				1	S-V
Pinaceae	*Pinus* spp.	2	1												½	3	S-V
Ranunculaceae	*Thalictrum* spp.							1	2		3	21	22	8½	6	9	S-V
Ranunculaceae	Sp.				1				1		1						S-V
Salicaceae	*Populus*															1	S-VI
Saxifragaceae	*Saxifraga* spp.											1		½			S-VI
Scrofulariaceae	*Verbascum*										2				½		S-VI
Ulmaceae	*Ulmus*	1															S-VI
Trilete spores			1														S-VI
Unidentified pollen		3	1		1							3		1	½	5	S-VI
Plant remains																	
Phytoliths								1	1		3	1			½		S-III
Trichomes													1				S-III

Table 4: *Amount and type of pollen, spores and plant remains found in ~⅛ filter for each air sample. * ~ ¼ filter is used for samples A2 and A3, which are therefore corrected to amounts comparable to ~ ⅛ filter. Absolute numbers per m^3 are calculated and presented in Figure 4C.*

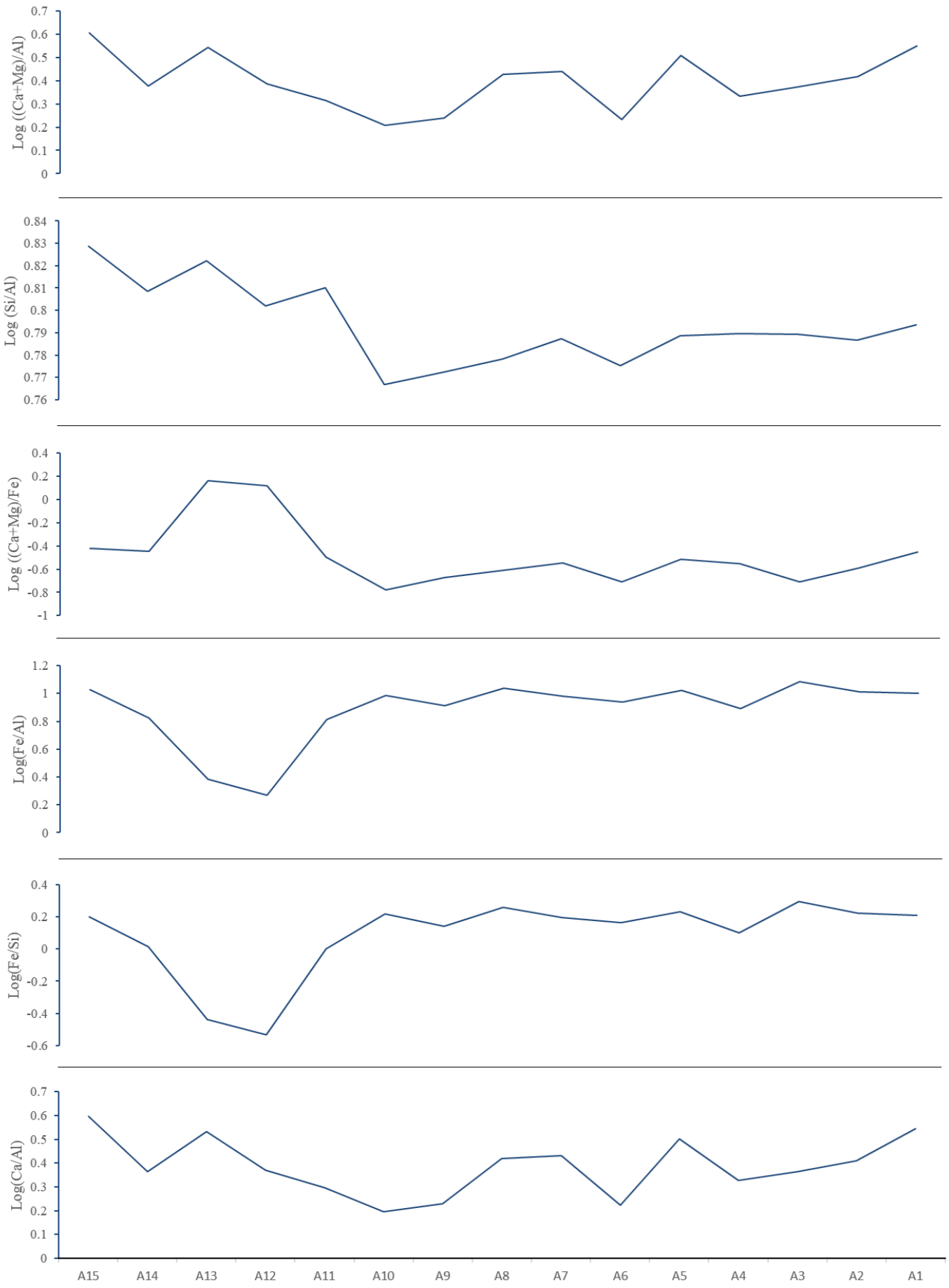

Figure 6: *XRF-measurements visualised for the ratios of Si/Al, (Ca+Mg)/Fe, Fe/Al, Ca/Al, Fe/Si and (Ca+Mg)/Al. All elements used for this figure are measured with 10 Kv.*

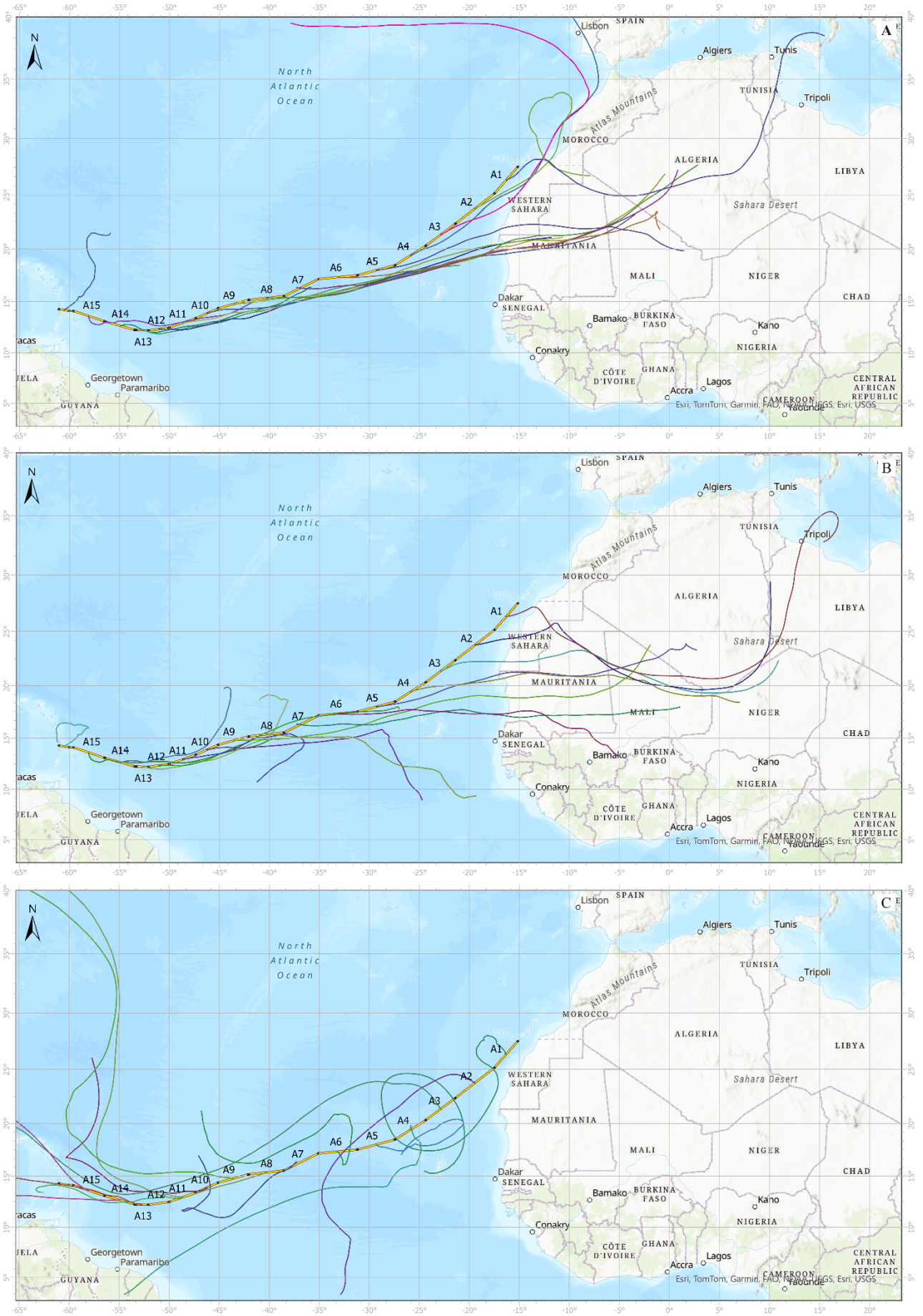

Figure 7: *Three maps showing the results from 5-day back trajectories (HYSPLIT) calculated backwards from the middle of each sample section, starting at;* ***(A)****: 8 m above sea level;* ***(B)****:500 m above sea level;* ***(C)****: 5000 m above sea level.*

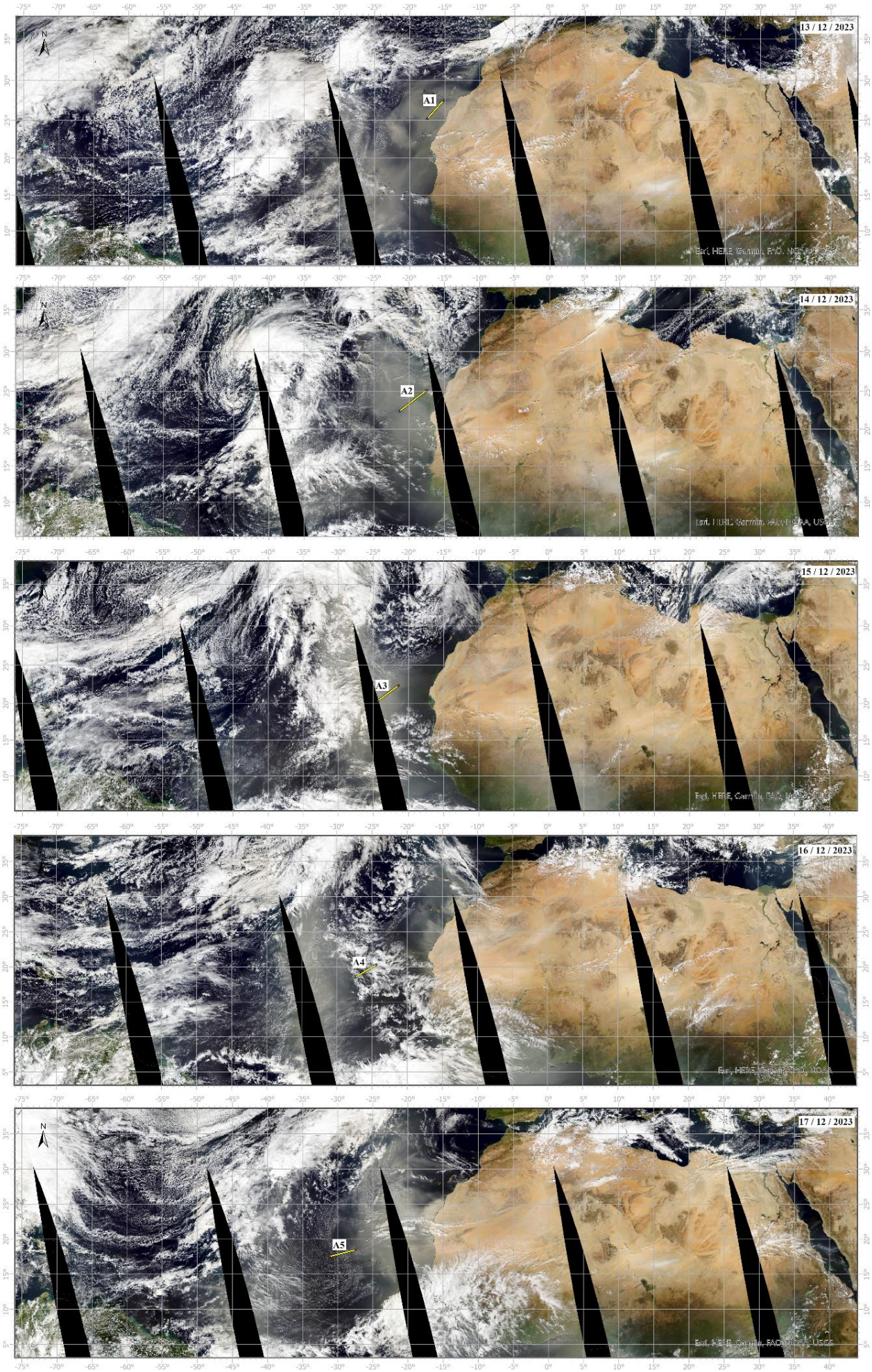

Figure 8: *Satellite images (EOSDIS) showing the pathway of major dust outbreaks from 13/12/2023 – 27/12/2023. Timing of the images coincides on average with the first few hours of each corresponding sample section.*

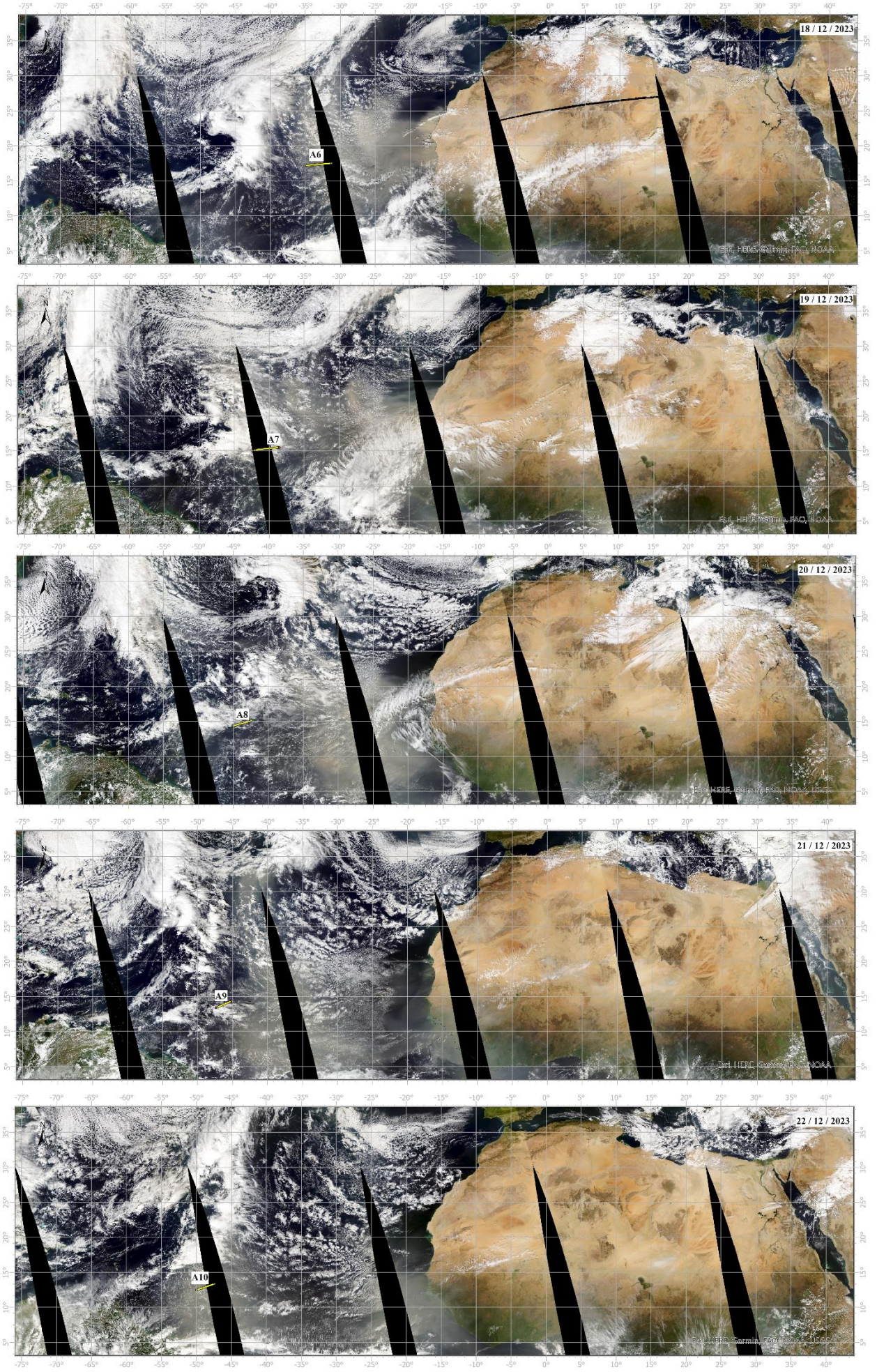

Figure 8 *(Continued)*

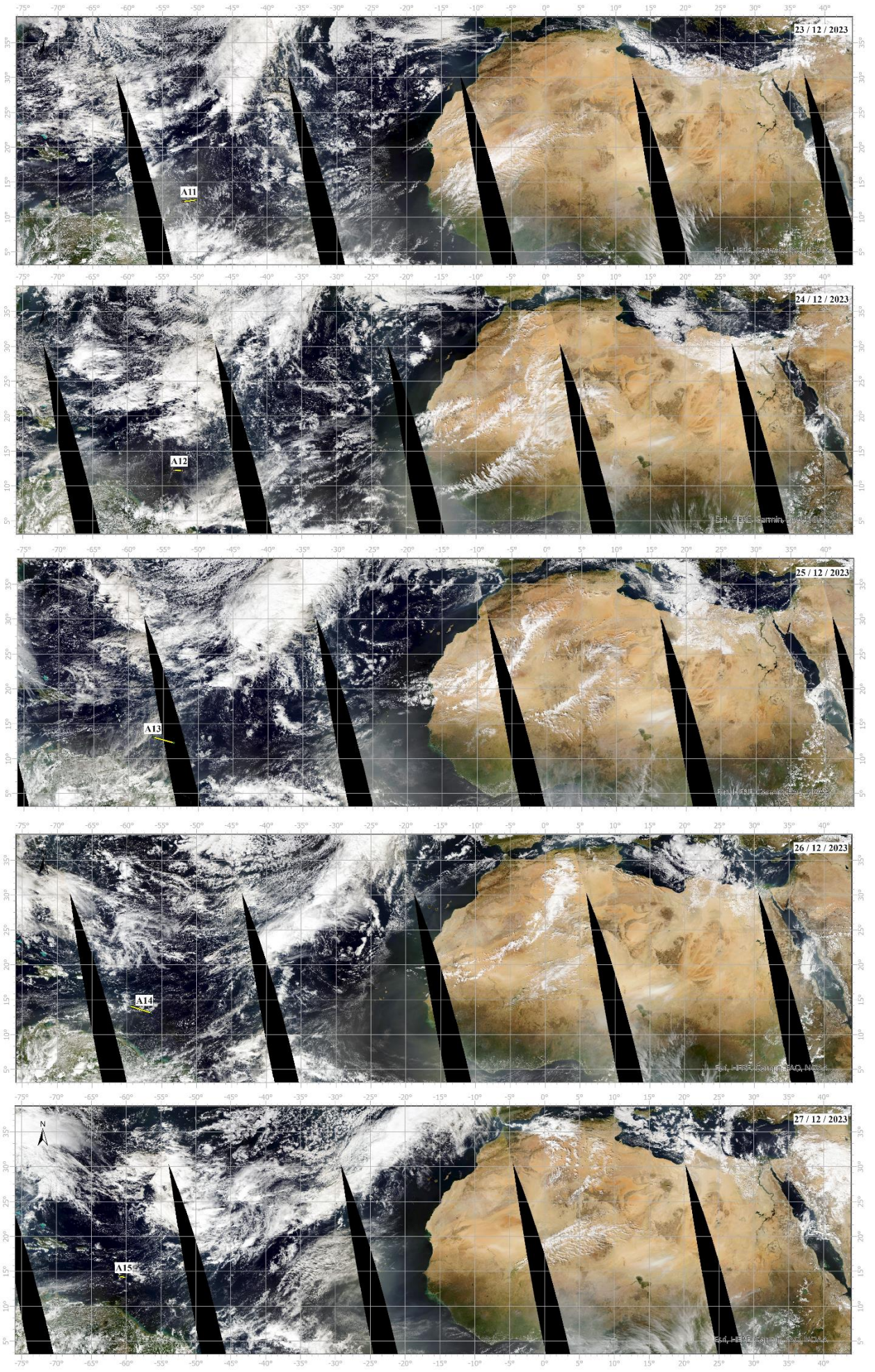

Figure 8 *(Continued)*

5. Discussion

5.1. Biological fraction

5.1.1. Diatom assemblage

The diatom assemblage in the dust samples predominantly consists of freshwater diatoms, with some specimens reaching as far as the Caribbean (Table 3). Most diatoms however do not reach this far, and the overall assemblage shows a gradual decline after about a third across the Atlantic Ocean (sample A5), and does not concur with changes in wind speed or wind direction (Table 2). The taxa *Aulacoseira ambigua, Aulacoseira granulata, Epithemia* spp., *Melosira* sp. and *Stephanodiscus* sp. are the most common within these dust samples, which is largely consistent with results from previous studies (Ehrenberg, 1847; Gasse et al., 1989 and references therein; Moreno et al., 2006; Barkley et al., 2021). Especially the presence of *Aulacoseira* spp. is significant, with an average abundance of 95%, and the genus is characteristic for most modern lakes and large rivers across North Africa (Foged, 1966; Talling, 1980; Gasse et al., 1989). Nevertheless, previous studies suggest that large quantities of such freshwater diatoms within major dust plumes most likely originate from African paleolakes due to the easily deflated nature of the low density sediments containing these diatoms (e.g., Gasse et al., 1989; Washington et al., 2006; Bristow et al., 2009; Barkley et al., 2021; Jewell et al., 2021). Multiple paleolakes in North Africa contain such diatom-rich surface sediments or extensive diatomite deposits and some are known to be active dust sources (Gasse et al., 1989; Gasse, 2002; Moreno et al., 2006; Bristow et al., 2009; Lécuyer et al., 2016; Barkley et al., 2021; Jewell et al., 2021). While these diatom rich surface sediments are relatively widespread in North Africa, only two regions known for substantial dust production have significant diatomite deposits that match the diatom assemblage obtained in this study; the paleolakes located at the tri-border area of Algeria, Mali and Niger in SA1 (see Figure 1) (with emphasis on the location known as the I-n-Atei paleolake) and paleolake Megachad located in SA2 (mainly the Bodélé Depression and paleoriver systems such as the Bahr El Gazel) (Gasse et al., 1989; Bristow et al., 2009; Lécuyer et al., 2016; Jewell et al., 2021). Nonetheless, since paleolakes are widespread across the entire Sahara and Sahel, other major dust sources containing a similar diatom assemblage may exist (Gasse et al., 1989; Gasse, 2002), however have not been reported in the literature so far.

Paleolake Megachad is by far the largest of the two regions (at least 350.000 km^2; Schuster et al., 2005; Drake & Bristow, 2006), is home to the largest single dust producing region of the world (the Bodélé depression) (Engelstaedter et al., 2006; Bristow et al., 2009; Evan et al., 2015), and has a diatom assemblage that closely resembles the diatoms obtained in this study (e.g., Gasse et al., 1989 and references therein; Moreno et al., 2006; Bristow et al., 2009). In comparison, the paleolakes located near the borders of Algeria, Mali and Niger are much smaller and the diatomite deposits remain relatively understudied with regards to their diatom assemblage. The exception to this is the I-n-Atei paleolake, which contains a rather similar diatom assemblage compared to the one obtained in this study (Gasse et al., 1989; Lécuyer et al., 2016). While the diatom assemblage from paleolake Megachad appears to display a stronger relation, the diatomite deposits at the tri-border area (like in the I-n-Atei paleolake) remain relatively understudied and the limited data therefore only provides snapshots from its complete diatom assemblage. Therefore, the assemblages from paleolakes at the tri-border area of Algeria, Mali and Niger potentially correspond better with the data obtained in this study than currently recognized and more research on these paleolakes is needed in order to compare their assemblages with more certainty.

5.1.2. Pollen assemblage

The large variety of pollen taxa observed in the dust samples from the west coast of Africa until about halfway across the Atlantic Ocean mainly represent the Mediterranean zone, the Steppe zone and the Sahara zone (Figure 2). Pollen

taxa representative for vegetation zones south of the Sahara zone (e.g., *Combretum, Mitracarpus, Alchornea* and *Elaeis*) are not represented in the dust samples obtained by this study. The minor downwind increase and taxa change for the most western samples (A14 - A15) is difficult to substantiate, since the identified pollen taxa are widespread and could originate from both the Caribbean region as well as Europe. Nonetheless, the change for samples A14 - A15 is interpreted to represent a more significant signal from the Caribbean or the Americas, due to the concurrent change in wind direction (Table 2) in combination with a close proximity to that region.

Especially *Artemisia*, Cyperaceae and *Thalictrum* are abundant in the first samples until about halfway across the Atlantic Ocean (Table 4) and are the main confirmation of the influence of the Mediterranean zone, the Steppe zone and the Sahara zone in these dust samples. *Artemisia* is moderately present in the dust samples and is a dominating element in the Steppe zone, abundant in the Sahara zone and abundant in the elevated areas of Algeria (Dupont. 1999; Gajewski et al., 2002; Hooghiemstra et al., 2006). Chenopodiaceae-Amaranthaceae and *Ephedra* are also characteristic for both the Steppe and Sahara zone (Dupont. 1999; Gajewski et al., 2002; Hooghiemstra et al., 2006). However, the Chenopodiaceae-Amaranthaceae in these dust samples most likely indicate a stronger influence from the Steppe zone, since the flowering season for this genus lies between July and September for the Sahara zone against November and April for the Steppe zone (Dupont. 1999; Gajewski et al., 2002). *Thalictrum* is not typically present in most vegetation zones of North Africa and indicates a signal from southern Europe or the most northern regions of Africa, clearly recording the influence of the northeast trade winds (Ziman & Keener, 1989). Although the abundance of *Thalictrum* suggests a signal from the northern zones, other pollen characteristic for these regions remain low in quantity, with only small numbers of *Pinus* and *Alnus* possibly originating from these regions. The small number of *Pinus* are however more likely dispersed from the pine forests located on the Canary Islands. This is because the Canary Islands are known to load the atmosphere with *Pinus* pollen and high concentrations of *Pinus* have been found in the marine surface sediments surrounding these islands (Hooghiemstra et al., 2006). However, the actual low concentration of *Pinus* obtained in this study is therefore rather notable and requires future attention. Cyperaceae is the most abundant in almost all dust samples and can be found in multiple zones, but especially in wetlands and coastal regions (e.g., Bryson & Carter, 2008; Simpson et al., 2011). Cyperaceae is usually accompanied by Poaceae pollen, which are also abundant in most North African climates, mainly in the Sahel zone (Dupont, 1999; Hooghiemstra et al., 2006). The lack of Poaceae and the distinct abundance of Cyperaceae in the dust samples therefore supports the minimal influence from the Sahel zone, and likely indicates the influence of wetlands, lakes or rivers near the source or along the pathway of the dust. The absence of Poaceae could also possibly reflect a difference in flowering phases or horizontal transporting distance. Nevertheless, considering the presence of pollen from various vegetation zones, the total absence of Poaceae in this study remains notable and requires additional attention in future studies as well. Finally, the phytoliths obtained in this study (mainly abundant in Poaceae and Cyperaceae) could originate from the Sahel zone, since savannah fires within this region are known to contribute to the release of large quantities of phytoliths in the air (Pokras & Mix, 1985; Romero et al., 2003). However, as the phytoliths remain unidentified and could be produced by various plant taxa, not only Poaceae and Cyperaceae (Barboni et al., 1999; Piperno, 2001), and other signals from the Sahel zone remain absent, interpretations connecting the phytoliths to this zone should be considered carefully.

5.1.3. Paleo- and modern-day indicators

Whether the biological fraction either consists of paleo-indicators or modern-day taxa is rather difficult to state with complete certainty. Previous studies suggest that the majority of atmospheric pollen off the west coast of Africa are freshly emitted (e.g., Calleja et al., 1993), and this is supported by the large amount of cellular content preserved within the obtained pollen. This however does not preclude the possibility that some pollen originate from the same

sedimentary paleo-lake deposits as is anticipated for the diatoms. Such a paleo-source contains various lacustrine sediments deposited during distinctly different environmental circumstances (e.g., a wetter climate), and therefore potentially explains the large numbers of aquatic pollen species observed in this study. The simultaneous decline in pollen and diatoms could substantiate this, since it possibly suggests a similar travelling distance for both biological assemblages. Nevertheless, other pollen indicative for different paleo-environmental conditions during pollen production should have been observed in that case as well. Moreover, the high concentration of cellular content further suggests that the pollen assemblage is unlikely to originate from such a paleo-source. Therefore, even though a paleo-source should not be completely disregarded, most pollen obtained in this study are considered to be freshly emitted.

Such caution also applies to the diatom assemblage obtained in this study. While the diatoms are interpreted to originate from African paleo-lake deposits, the high percentage of cellular content within the *Aulacoseira* genera (Table 3) could be an indication for a modern source, such as rivers or lakes. Nonetheless, a paleo-origin for the diatom assemblage is supported by the corresponding diatom assemblages from various paleo-lake deposits (see section 5.1.1), as well as the presence of species like *Eunotia pierrefuseyi,* which most likely indicate tropical circumstances during deposition (Taylor et al., 2016; Cocquyt, 2020). An identification on species level of the *Stephanodiscus* genera collected in this study could provide confirmation regarding a paleo-source as the primary contributor, since recognition of species like *S. carconensis, S. transylvanicus* and *S. niagarae* would directly support Pliocene and Pleistocene sediments of Chadian and Algerian paleo-lakes as potential sources (Fourtanier & Gasse, 1988; Gasse et al., 1989). Therefore, further research is needed in order to determine whether the diatom assemblage in the dust samples originates from paleo-lake sediments, from modern-day lakes and rivers, or indicates a mixture of paleo- and modern-day sources.

5.2. Downwind characteristics

5.2.1. Downwind characteristics in concentration

The change in dust concentrations observed in this study demonstrate an overall decline in concentration further west (Figure 4b), which corresponds with the results from previous studies (e.g., Van der Does et al., 2020). However, this decline only initiates after about two thirds across the Atlantic Ocean (sample A9), which is in contrast to the expectations that the low altitude winter winds deposit most of the dust close to the African coast (Pye, 1987). Moreover, the lower concentrations for samples A2 - A3 and the minor increase from samples A6 - A8 are clear deviations from this general trend observed in dust concentration.

The minor increase in concentration for samples A6 - A8 occurs during a slight amplification in absolute wind speed (Table 2), which possibly explains this minor increase. An alternative explanation for such an increased concentration could be a local displacement or change within the source location. Nevertheless, this is considered less likely since a distinct change in composition (e.g., pollen, diatoms, grain size) would then be expected as well, which is not observed. Therefore, since the change in concentration is only minor and is unlikely to indicate a change at the source, it is most likely the result of the minor change in wind speed. Another contrasting observation for these samples, is the visual absence of a dust plume over the sampling route concurrent with the maximum dust concentration for sample A8 (Figure 8). This is interpreted to indicate a lower concentration of aerosols in the upper atmospheric layers, while aerosol concentrations at lower elevations remain relatively unchanged.

In contrast to samples A6 - A8, the distinct drop in concentration for samples A2 - A3 does not coincide with changes in absolute wind speed. Moreover, the satellite images demonstrate complete or partial covering by dust plumes for these samples (Figure 8). The discordance between this significant decrease in concentration and the visible presence

of major dust plumes may once again be linked to variations in aerosol concentration at various altitudes. The drop in concentration could be explained by a change in source location, however, a distinct change in the assemblage and amount of the diatoms would then be anticipated as well, which is not observed. Therefore, since changes in aridity at the source location can directly affect the amount of dust dispersion (e.g., Pye, 1989; Hesse, 1994; Arimoto, 2001; Palchan & Torfstein, 2019), this sudden decrease in dust concentration is interpreted to reflect less arid conditions at the source location and, therefore, possibly records a minor local displacement or change within the dominant source location.

Finally, while the dust concentration for sample A4 accommodates again to the general trend, a significant change in the comparative amount of diatoms can be observed. This sample contains almost half of the respective diatom concentration compared to samples A1, A2, A3 and A5 (Figure 4b and 4c). Nevertheless, the diatom assemblage observed for sample A4 remains unchanged (Table 3). Therefore, this samples is also interpreted to signal a minor shift within the dominant source location, and, due to the similar diatom assemblage, not a complete displacement of source locations. Nevertheless, as mentioned in the method section, interpretations based on the absolute quantity of the biological fraction in this study should be considered with caution.

5.2.2. Downwind characteristics in grain size

The results from the grain-size analysis demonstrate notably small median grain sizes between 3 and 5 µm and overall minor downwind changes (Figure 5). These observations do not align with the observations from previous studies (e.g., Van der Does et al., 2016; Van der Does et al., 2021), or with the higher settling velocity for larger particles. The small median grain sizes and minimal downwind changes are interpreted to be the result of the large amount of diatoms observed in the samples during the first half of the sampling route. Even though most of the observed diatoms are considerably large contrasted with the small grain sizes of the dust samples (see Plate S-I), the substantial amount of diatoms are the only significant difference in comparison with previous studies. Moreover, the results from the redundancy analysis (presented in section 5.3.) support this by indicating a negative relation between the median grain sizes and the amount of diatoms. Because of this, no elaborate comparison can be made to the results of grain-size analyses presented in previous studies. Why the laser particle sizer generates such smaller grain sizes as a result of more and larger diatom fragments remains unanswered. Therefore, attention to observations of such signals is recommended for future studies.

A slightly wider grain-size distribution compared to the general trend can be observed in Figure 5a for samples A1 – A5 and A12 - A13 (Figure 5a). Such a wider distribution could indicate a higher abundance of monomineral particle fragments (primary minerals) compared to clay mineral aggregates (Stuut et al., 2009). A higher abundance of monomineral particle fragments is however more likely the case for samples A1 – A5 than for samples A12 - A13. This is because previous studies indicate a relative downwind increase in clay minerals (e.g., Glaccum & Prospero, 1980; Goudie & Middleton, 2006), a pattern that is also observed in this study (see section 5.2.3.). Alternatively, the higher concentration of relatively large diatoms in the first samples (Plate S-I; Plate S-II; Figure 4) could possibly attribute to the wider range in size distribution for samples A1 – A5 as well. However, the relative diatom concentration of sample A4 is comparable to sample A6, which displays a narrow grain-size distribution similar to samples A7 - A10. Therefore, the wider signal observed for A1 – A5 is mainly interpreted to indicate a higher abundance of monomineral particle fragments compared to clay mineral aggregates.

In contrast, the wider distribution and larger grain sizes observed for samples A12 - A13 diverge from the results of previous studies (Koopmann, 1979; Weltje & Prins, 2003; Holz et al., 2004; Van der Does et al., 2016) and from the relative downwind increase in clay minerals observed in this study (section 5.2.3.). This wider signal might be related

to the decision of using a magnetic stirrer to separate the dust particles during particle analysis instead of chemical reagents. Clay particles, which are interpreted to be more abundant in samples A12 - A13 (see section 5.2.3), could therefore possibly stick together and result in a coarser and wider signal. Alternatively, the observed decline in wind speed could possibly stimulate larger particles suspended higher up in the atmosphere to descend, resulting in an overall wider grain-size distribution as well. Nevertheless, a concurrent decline in relative Fe-concentration (see section 5.2.3) displays a distinctive different signal compared to the other samples, and samples A12 - A13 are therefore considered to reflect a displacement of the dominant source location.

The coarse shoulders observed for samples A4, A5 and A11 in Figure 5a clearly deviate from the general trend and are not observed in other samples. The shoulder at sample A11 is interpreted to reflect a relative increase in platy clay minerals, which the particle sizer may misread due to their platy shape and therefore report larger sizes than the actual grain sizes (Stuut et al., 2005; Korte, 2018). Such a signal coupled to a relative increase in platy clay minerals would be consistent with the results from Glaccum and Prospero (1980) and, more recently, the results by Van Der Does et al. (2018). This is most likely not the case for samples A4 and A5, which are expected to have a relatively low abundance of clay mineral aggregates due to the short traveling distance for dust to the sampling location. This is also supported by the ratio of Si/Al, which shows no distinct deviations in the relative abundance of clay minerals for these samples (Figure 6). Other potential causes, like significantly more pollen or diatoms, are not observed as well. In fact, sample A4 actually contains almost half of the respective diatom concentration compared to similar samples. Therefore, the exact cause for the shoulders observed for samples A4 and A5 remain unresolved.

5.2.3. Downwind characteristics in bulk chemical composition

Due to the semi-quantitative nature of the XRF-data, no direct comparison could be made with the quantitative data used in most studies connecting chemical signals to source locations. Nevertheless, several notable trends in the bulk chemical data can be observed (Figure 6). For instance, the Ca/Al ratio demonstrates a modest parabolic pattern which appears rather similar to the trend observed in median grain sizes (Figure 5b). This is indeed anticipated, as higher values for Ca/Al are related to larger grain sizes (Zarasvandi, 2009). In contrast, the Si/Al ratio remains rather stable until sample A10 after which it shows a gradual downwind decline, suggesting a relative increase of clay minerals for samples A10 - A15 (e.g., Avila et al., 1997; Blanco et al., 2003). While no general trend can be observed for Fe, the significant change in ratios (Ca+Mg)/Fe, Fe/Si and Fe/Al for samples A12 - A13 suggests a substantial decrease in Fe-concentration for these samples. This decline in Fe appears concurrent with the increased grain size and wider grain-size distribution for samples A12 - A13 (Figure 5a)(section 5.2.2.), and is also considered to represent the displacement of the dominant source location as interpreted for these samples. Finally, while Ca and Mg are distinctive for different source regions across North Africa (Scheuvens et al., 2013), no significant interpretations can be deduced from their signals.

5.3. Redundancy analyses

Two RDA analyses are applied and examined to verify the similarity between the dust samples and to test the influence of environmental variables on response variables. In this work, the response variables are defined as data-sets that are possibly affected by the considered environmental variables. Selected response variables are therefore dust concentration and median grain size, but also concentrations of diatoms, pollen and fungi spores, and specific genera of the biological fraction that are dominant in the dust samples. The considered environmental variables include the distance to the African coast and changes in air pressure and wind speed. Response variables are divided over two analyses to facilitate the interpretation; with analysis 1 showing dust concentration, median grain size and

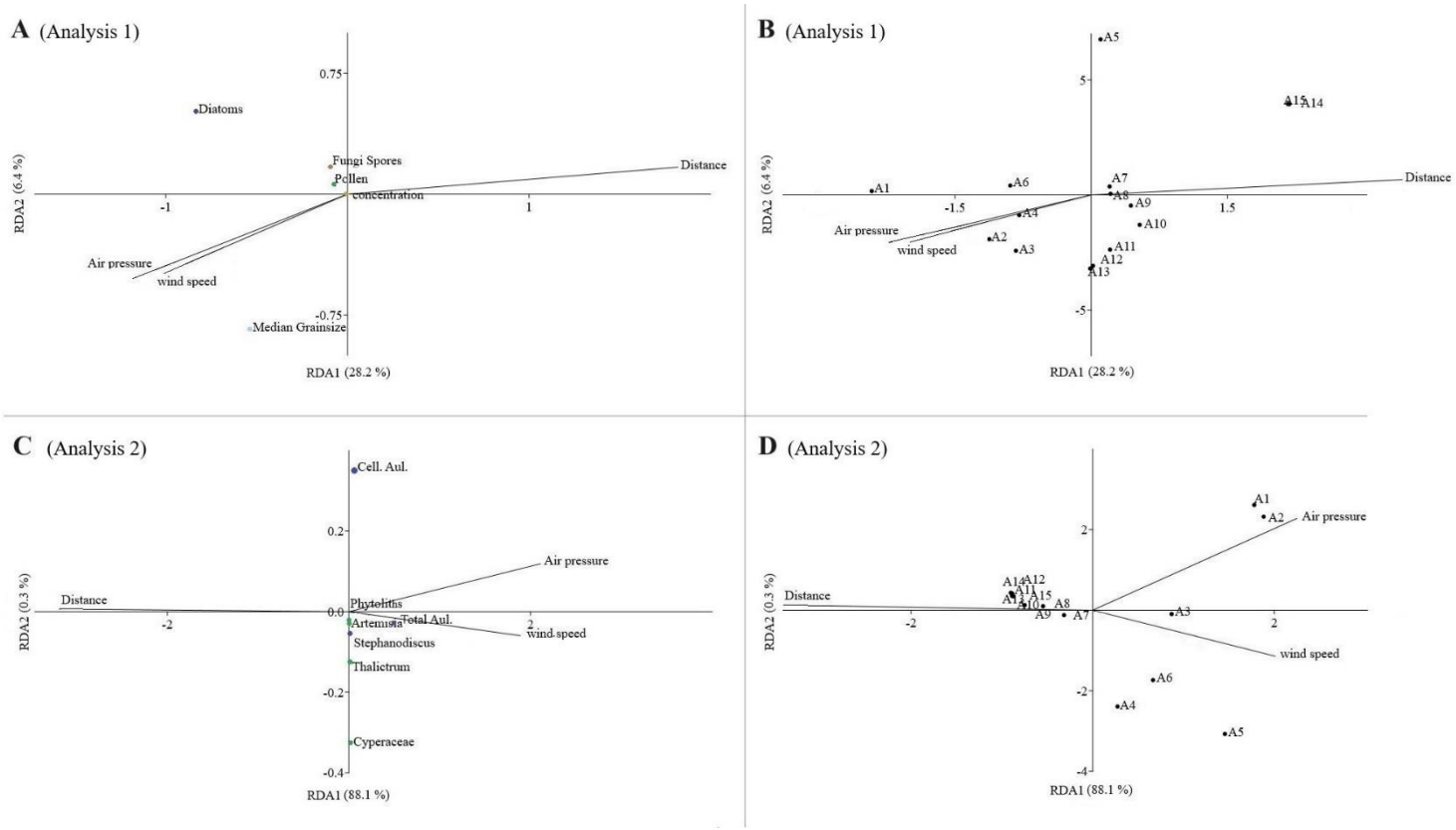

Figure 9: *Results of the RDA analyses:* ***(A)****: Plot of analysis 1 showing the response variables (as dots) of dust concentration, median grainsize and concentrations of diatoms, fungi spores and pollen against the environmental variables (as lines) of air pressure, distance to the African coast and wind speed;* ***(B)****: Plot of analysis 1 showing the distribution of the sample points (N=15) based on the response variables of (A) against the environmental variables of air pressure, distance to the African coast and wind speed;* ***(C)****: Plot of analysis 2 showing response variables (as dots) of Artemisia, cellular Aulacoseira, Cyperaceae, phytoliths, Stephanodiscus, Thalictrum and total Aulacoseira against the environmental variables (lines) of air pressure, distance to the African coast and wind speed;* ***(D)****: Plot of analysis 2 showing the distribution of the sample points (N=15) based on the response variables of (C) against the environmental variables of air pressure, distance to the African coast and wind speed.*

concentrations of diatoms, pollen and fungi spores, and analysis 2 showing changes in the dominant genera of the biological fraction. The results of the RDA analyses are provided in Figure 9.

The result of analysis 1 shows a positive relation along axis RDA1 (explaining 28.2 % of the variance) between the amount of diatoms, median grain size, fungi spores and pollen and the environmental variables of wind speed and air pressure (Figure 9a). In contrast, a negative relation is observed between these response variables and the distance to the African coast, and no relation is observed between the dust concentration and any environmental variable. Especially the amount of diatoms and changes in median grain size seem to respond strongly to changes in the environmental variables. Moreover, the data on diatoms and median grain size are negatively related to each other along axis RDA2 (explaining 6.4 % of the variance). Although this axis only explains a minor part of the observed variance, the negative relation is striking since most of the observed diatoms are considerably larger than the measured grain sizes of the dust samples (see Plate S-I). This supports the interpretation that the large amount of diatoms observed in the dust samples affect the outcome of the grain-size analysis (section 5.2.2.). Furthermore, analysis 1 shows the results obtained from samples A1 - A4 and A6 to be influenced by air pressure and wind speed, whereas the results obtained from samples A5 and A7 - A12 are influenced by distance to the African coast (Figure 9b). The results obtained from samples A12 - A13 show no relation to the considered environmental variables at all. This is consistent with the interpretation that the significant differences observed for samples A12 - A13 (see sections 5.2.2. and 5.2.3.) are caused by a change in source location and not by changes of environmental variables. Samples

A14 - A15 are also tightly clustered and are significantly influenced by the distance variable compared to the other samples, supporting the interpretation that the dust in these samples partially originate from the Americas.

Most response variables in analysis 2 show a minimum to no correlation to any environmental variables along axis RDA1 (explaining 88.1 % of the variance) (Figure 9c). Only the concentration of total *Aulacoseira*, and in part the cellular *Aulacoseira*, show a positive relation to air pressure and wind speed and a negative relation to distance. In contrast, a clear difference is shown along axis RDA2 (explaining 0.3 % of the variance) and appears largely unrelated to the environmental variables considered in this analysis. The differences along axis RDA2 could therefore possibly relate to the origin of these biological fragments. However, given that this axis explains only a minor portion of the variance (0.3%), any interpretations regarding the underlying causes of these differences should be approached with caution. Furthermore, analysis 2 shows the results obtained from samples A7 - A15 to be tightly clustered, to correlate positively with distance and to correlate negatively with air pressure and wind speed (Figure 9d). Both analyses show similar results, which indicates that samples A1 - A6 are more likely to be affected by environmental variables like wind speed, while after sample A6 the distance to the origin of the source becomes one of the dominant factors for changes in composition and grain size.

5.4. Potential source regions

Of the three major potential source regions as described by Jewell et al. (2021), only two regions share characteristics that correspond with the obtained dataset in this study; SA1 and SA2. Overall, a higher probability for the dominance of source area SA1 compared to SA2 (figure 1) is interpreted for the trans-Atlantic transport of dust at the moment of data collection. While the diatoms in this study are most similar to the diatom assemblage dispersed from paleolake Megachad in SA2, its unlikely influence is supported by; the absence of the AEJ, a larger distance to the western coast, an absence of Sahelian pollen, and finally, the dominance of the Harmattan winds in this region transporting dust to the southwest, away from the sampling locations. In contrast, the active dust sources located in SA1 are much closer to the western coast and are more in line with the northeastern trade winds and the sampling locations. Moreover, SA1 encompasses the tri-border area of Algeria, Mali and Niger, the region where paleolakes dominate dust production and which is considered to be the second most active dust source in Africa (Evan et al., 2015).

Both the pollen and diatom assemblages obtained by this study support the possible dominance of the tri-border region of Algeria, Mali and Niger, and most of the retraced pathways from the HYSPLIT model support this as well (Figure 7). Although the dust plumes visible on the satellite images (Figure 8) are harder to interpret above land, the satellite images do not show any significant deviations from this interpretation. If the sedimentary deposits of paleolake Megachad are indeed not a dominant factor in these dust samples, as interpreted, emphasis should be given to the role of the paleolakes near the tri-border area of Algeria, Mali and Niger as the dominant dust producing region during boreal winter and as source for diatoms-rich dust to the Atlantic Ocean.

6. Conclusions

The primary objective of this study is to explore downwind changes in North African dust emissions across the Atlantic Ocean during boreal winter, with an emphasis on compositional characteristics and origin. For this, the results of trans-Atlantic dust samples are analysed and interpreted. The following compositional characteristics and significant downwind changes are observed:

- In general, high dust concentrations of ~ 0.03 mg m^{-3} day^{-1} are reported for the first major part of the sampling route, and after about two thirds across the Atlantic Ocean dust concentrations decline to about 0.002 mg m^{-3} day^{-1}.
- High concentrations of freshwater diatoms are observed for approximately the first half of the sampling route (~ 2 diatoms per m^3) and remain present to as far as the Caribbean region. Especially *Aulacoseira ambigua*, *Aulacoseira granulata*, *Epithemia* spp., *Melosira* sp. and *Stephanodiscus* sp. are dominant species and genera, with *Aulacoseira* representing ~ 95 % of all observed diatoms.
- The pollen assemblage obtained in this study indicates an influence from the Mediterranean zone, the Steppe zone and the Sahara zone until about two thirds of the sampling route.
- A relatively higher concentration of monomineral particle fragments is observed for samples closer to the African coast, against a relatively higher concentration of clay minerals for samples closer to the Caribbean.
- Downwind variations in grain size, although remarkably small, demonstrate a gradual decline for the first half of the sampling route, after which little variation occurs until the final third of the sampling route. The last part of the sampling route is characterized by a minor increase in median grain size from ~ 3 μm to ~ 4.5 μm, resulting in similar grainsizes between the most western and eastern samples.

The majority of the obtained dust samples is interpreted to originate from a major area encompassing northern Mauritania, northern Mali, north-western Niger and southern Algeria (SA1 - Figure 1). Within this region, a specific dominance is interpreted from the paleolakes at the tri-border region of Algeria, Mali and Niger. Samples A2 - A3 and A4 are interpreted to signal a minor local displacement within this source region, whereas the results from samples A12 - A13 indicate a major source displacement within North Africa. In contrast, the two most western samples (A14 - A15) indicate an influence from the Caribbean region or the Americas. Finally, further research is suggested on the diatom assemblage of the paleolakes at the tri-border region of Algeria, Mali and Niger in order to correlate diatom-rich dust samples from future studies to these paleolakes with more certainty. As the tri-border region of Algeria, Mali and Niger is currently not recognized as an important source for diatom-rich dust, future emphasis should be given to the role of this region in providing significant elevated concentrations of diatoms for trans-Atlantic dust transport during winter.

Acknowledgements

Special thanks to Timme Donders, Francesca Sangiorgi and Jan-Berend Stuut for supervising this project, with added appreciation to Jan-Berend Stuut for assisting with the XRF, grain-size and concentration data; Kees Nooren is thanked for his input into the project, assistance during microscope work and help in the laboratory; Reinoud van der Heijden for helping with the fieldwork logistics; Giovanni Dammers and Natasja Welters for assistance in the laboratory; and captain, crew and guests aboard the Stad Amsterdam for their interest in the project and assistance with logistics and data-collection, with special thanks to Coert Kool, Fleur Nooteboom, Gary Maynard, Kristina Kinsman Maynard, Peronel Barnes and Tim Gorter. The Royal Netherlands Institute for Sea Research (NIOZ) is thanked for lending of the dust sampler and Alexander Hoogenboom and Mariska Hoorweg for providing the additional materials used during fieldwork. The Hofvijferkring foundation and Utrecht University are thanked for financial support, without which this project would not have been possible.

References

Adams, A. M., Prospero, J. M., & Zhang, C. (2012). CALIPSO-derived three-dimensional structure of aerosol over the Atlantic Basin and adjacent continents. Journal of Climate, 25(19), 6862-6879.

Arimoto, R. (2001). Eolian dust and climate: relationships to sources, tropospheric chemistry, transport and deposition. Earth-Science Reviews, 54(1-3), 29-42.

Avila, A., Queralt-Mitjans, I., & Alarcón, M. (1997). Mineralogical composition of African dust delivered by red rains over northeastern Spain. Journal of Geophysical Research: Atmospheres, 102(D18), 21977-21996.

Bakker, N. L., Drake, N. A., & Bristow, C. S. (2019). Evaluating the relative importance of northern African mineral dust sources using remote sensing. Atmospheric Chemistry and Physics, 19(16), 10525-10535.

Barboni, D., Bonnefille, R., Alexandre, A., & Meunier, J. D. (1999). Phytoliths as paleoenvironmental indicators, west side Middle Awash Valley, Ethiopia. Palaeogeography, Palaeoclimatology, Palaeoecology, 152(1-2), 87-100.

Barkley, A. E., Olson, N. E., Prospero, J. M., Gatineau, A., Panechou, K., Maynard, N. G., ... & Gaston, C. J. (2021). Atmospheric transport of North African dust-bearing supermicron freshwater diatoms to South America: Implications for iron transport to the equatorial North Atlantic Ocean. Geophysical Research Letters, 48(5), e2020GL090476.

Ben-Ami, Y., Koren, I., Altaratz, O., Kostinski, A., & Lehahn, Y. (2012). Discernible rhythm in the spatio/temporal distributions of transatlantic dust. Atmospheric Chemistry and Physics, 12(5), 2253-2262.

Blanco, A., Dee Tomasi, F., Filippo, E., Manno, D., Perrone, M. R., Serra, A., ... & Tepore, A. (2003). Characterization of African dust over southern Italy. Atmospheric Chemistry and Physics, 3(6), 2147-2159.

Bristow, C. S., Drake, N., & Armitage, S. (2009). Deflation in the dustiest place on Earth: the Bodélé Depression, Chad. Geomorphology, 105(1-2), 50-58.

Bristow, C. S., Hudson-Edwards, K. A., & Chappell, A. (2010). Fertilizing the Amazon and equatorial Atlantic with West African dust. Geophysical Research Letters, 37(14).

Bryson, C. T., & Carter, R. (2008). The significance of Cyperaceae as weeds. Sedges: uses, diversity, and systematics of the Cyperaceae, 108, 15.

Calleja, M., Rossignol-Strick, M., & Duzer, D. (1993). Atmospheric pollen content off West Africa. Review of Palaeobotany and Palynology, 79(3-4), 335-368.

Cocquyt, C. (2020). Correction of the type locality of Eunotia leonardii JC Taylor, Cocquyt & Mayama and Eunotia pierrefuseyi JC Taylor & Cocquyt (Eunotiaceae, Bacillariophyceae) from DR Congo. Phytotaxa, 245(3), 187-196.

Cole, J. M., Goldstein, S. L., demenocal, P. B., Hemming, S. R., & Grousset, F. E. (2009). Contrasting compositions of Saharan dust in the eastern Atlantic Ocean during the last deglaciation and African Humid Period. Earth and Planetary Science Letters, 278(3-4), 257-266.

Creamean, J. M., Suski, K. J., Rosenfeld, D., Cazorla, A., DeMott, P. J., Sullivan, R. C., ... & Prather, K. A. (2013). Dust and biological aerosols from the Sahara and Asia influence precipitation in the western US. science, 339(6127), 1572-1578.

Claquin, T., Roelandt, C., Kohfeld, K., Harrison, S., Tegen, I., Prentice, I., ... & Schulz, M. (2003). Radiative forcing of climate by ice-age atmospheric dust. Climate Dynamics, 20, 193-202.

Darwin, C. (1846). An account of the Fine Dust which often falls on Vessels in the Atlantic Ocean. Quarterly Journal of the Geological Society, 2(1-2), 26-30.

Drake, N., & Bristow, C. (2006). Shorelines in the Sahara: geomorphological evidence for an enhanced monsoon from palaeolake Megachad. The Holocene, 16(6), 901-911.

Dupont, L. M. (1999). Pollen and spores in marine sediments from the east Atlantic-A view from the ocean into the African Continent. In Use of proxies in paleoceanography: Examples from the South Atlantic (pp. 523-546). Berlin, Heidelberg: Springer Berlin Heidelberg.

Ehrenberg, C. G. (1847). Passatstaub und Blutregen. Ein großes organisches unsichtbares Leben in der Atmosphare. Abhandlungen der Koniglichen Akademie der Wissenschaften zu Berlin, Physikalische-mathematische Klasse.

Engelstaedter, S., Tegen, I., & Washington, R. (2006). North African dust emissions and transport. Earth-Science Reviews, 79(1-2), 73-100.

Evan, A. T., Fiedler, S., Zhao, C., Menut, L., Schepanski, K., Flamant, C., & Doherty, O. (2015). Derivation of an observation-based map of North African dust emission. Aeolian Research, 16, 153-162.

Foged, N. (1966). Freshwater diatoms from Ghana.

Fourtanier, E., & Gasse, F. (1988). 1st records on lacustrine diatom biostratigraphy and evolution in Africa over 11 Ma. Comptes rendus de l academie des sciences serie II, 306(19), 1401-1408.

Friese, C. A., van der Does, M., Merkel, U., Iversen, M. H., Fischer, G., & Stuut, J. B. W. (2016). Environmental factors controlling the seasonal variability in particle size distribution of modern Saharan dust deposited off Cape Blanc. Aeolian research, 22, 165-179.

Gajewski, K., Lézine, A. M., Vincens, A., Delestan, A., & Sawada, M. (2002). Modern climate–vegetation–pollen relations in Africa and adjacent areas. Quaternary Science Reviews, 21(14-15), 1611-1631.

Gasse, F., Stabell, B., Fourtanier, E., & van Iperen, Y. (1989). Freshwater diatom influx in intertropical Atlantic: relationships with continental records from Africa. Quaternary Research, 32(2), 229-243.

Gasse, F. (2002). Diatom-inferred salinity and carbonate oxygen isotopes in Holocene waterbodies of the western Sahara and Sahel (Africa). Quaternary science reviews, 21(7), 737-767.

Glaccum, R. A., & Prospero, J. M. (1980). Saharan aerosols over the tropical North Atlantic—Mineralogy. Marine geology, 37(3-4), 295-321.

Gosling, W. D., Miller, C. S., & Livingstone, D. A. (2013). Atlas of the tropical West African pollen flora. Review of Palaeobotany and Palynology, 199, 1-135.

Goudie, A. S., & Middleton, N. J. (2001). Saharan dust storms: nature and consequences. Earth-science reviews, 56(1-4), 179-204.

Grousset, F. E., Parra, M., Bory, A., Martinez, P., Bertrand, P., Shimmield, G., & Ellam, R. M. (1998). Saharan wind regimes traced by the Sr–Nd isotopic composition of subtropical Atlantic sediments: last glacial maximum vs today. Quaternary Science Reviews, 17(4-5), 395-409.

Guiry, M., & Guiry, G. (2020). AlgaeBase. World-wide electronic publication. Natl Univ Ireland, Galway http.

Guo, C., Yu, J., Ho, T. Y., Wang, L., Song, S., Kong, L., & Liu, H. (2012). Dynamics of phytoplankton community structure in the South China Sea in response to the East Asian aerosol input. Biogeosciences, 9(4), 1519-1536

Hamilton, R. A., Archbold, J. W., & Douglas, C. K. M. (1945). Meteorology of Nigeria and adjacent territory. Quarterly Journal of the Royal Meteorological Society, 71(309-310), 231-264.

Hammer, Ø., & Harper, D. A. (2001). Past: paleontological statistics software package for educaton and data anlysis. Palaeontologia electronica, 4(1), 1.

Hesse, P. P. (1994). The record of continental dust from Australia in Tasman Sea sediments. Quaternary Science Reviews, 13(3), 257-272.

Holz, C., Stuut, J. B. W., & Henrich, R. (2004). Terrigenous sedimentation processes along the continental margin off NW Africa: implications from grain-size analysis of seabed sediments. Sedimentology, 51(5), 1145-1154.

Hooghiemstra, H., Lézine, A. M., Leroy, S. A., Dupont, L., & Marret, F. (2006). Late Quaternary palynology in marine sediments: a synthesis of the understanding of pollen distribution patterns in the NW African setting. Quaternary International, 148(1), 29-44.

IPCC (2013). Climate Change: The Physical Science Basis. Contribution of Working Group I to the Fifth Assessment Report of the Intergovernmental Panel on Climate Change, edited by: Stocker, . F., Qin, D., Plattner, G.-K., Tignor, M., Allen, S.

K., Boschung, J., Nauels, A., Xia, Y., Bex, V., and Midgley, P. M., Cambridge University Press, Cambridge, UK and New York, NY, USA, 1535 pp., 2013

Jewell, A. M., Drake, N., Crocker, A. J., Bakker, N. L., Kunkelova, T., Bristow, C. S., ... & Wilson, P. A. (2021). Three North African dust source areas and their geochemical fingerprint. Earth and Planetary Science Letters, 554, 116645.

Jickells, T. D., An, Z. S., Andersen, K. K., Baker, A. R., Bergametti, G., Brooks, N., ... & Torres, R. (2005). Global iron connections between desert dust, ocean biogeochemistry, and climate. science, 308(5718), 67-71.

Kalu, A.E. (1979). The African dust plume: its characteristics and propagation across West Africa in winter. In: Morales, C. (Ed.), Saharan dust: Mobilization, transport, deposition. John Wiley, New York

Karydis, V. A., Kumar, P., Barahona, D., Sokolik, I. N., & Nenes, A. (2011). On the effect of dust particles on global cloud condensation nuclei and cloud droplet number. Journal of Geophysical Research-Atmospheres, 116(GSFC-E-DAA-TN8102).

Klaas, C., & Archer, D. E. (2002). Association of sinking organic matter with various types of mineral ballast in the deep sea: Implications for the rain ratio. Global biogeochemical cycles, 16(4), 63-1.

Knippertz, P., & Stuut, J. B. W. (2014). Mineral dust. Mineral dust—A key player in the Earth system, 121-147.

Koopmann, B. (1981), Sedimentation von Saharastaub im subtropischen Nordatlantik wa¨hrend der letzten 25.000 Jahre, Meteor Forschungsergeb., Reihe C, 35, 23 – 59

Korte, L. F., Brummer, G. J., van der Does, M., Guerreiro, C. V., Hennekam, R., van Hateren, J. A., ... & Stuut, J. B. W. (2016). Compositional changes of present-day transatlantic Saharan dust deposition. Atmos. Chem. Phys, 17, 6023-6040.

Korte, L. F., Brummer, G. J. A., Van Der Does, M., Guerreiro, C. V., Hennekam, R., Van Hateren, J. A., ... & Stuut, J. B. W. (2017). Downward particle fluxes of biogenic matter and Saharan dust across the equatorial North Atlantic. Atmospheric Chemistry and Physics, 17(9), 6023-6040.

Korte, L. F. (2018). Saharan dust deposition in the equatorial North Atlantic Ocean and its impact on particle export fluxes.

Lécuyer, C., Lézine, A. M., Fourel, F., Gasse, F., Sylvestre, F., Pailles, C., ... & Barral, A. (2016). In-Atei palaeolake documents past environmental changes in central Sahara at the time of the "Green Sahara": Charcoal, carbon isotope and diatom records. Palaeogeography, Palaeoclimatology, Palaeoecology, 441, 834-844.

Li-Jones, X., & Prospero, J. M. (1998). Variations in the size distribution of non-sea-salt sulfate aerosol in the marine boundary layer at Barbados: Impact of African dust. Journal of Geophysical Research: Atmospheres, 103(D13), 16073-16084.

Littmann, T. (1991). Dust storm frequency in Asia: climatic control and variability. International Journal of Climatology, 11(4), 393-412.

Martínez-Garcia, A., Rosell-Melé, A., Jaccard, S. L., Geibert, W., Sigman, D. M., & Haug, G. H. (2011). Southern Ocean dust–climate coupling over the past four million years. Nature, 476(7360), 312-315.

McTainsh, G. (1980). Harmattan dust deposition in northern Nigeria. Nature, 286(5773), 587-588.

Melia, M. B. (1984). The distribution and relationship between palynomorphs in aerosols and deep-sea sediments off the coast of northwest Africa. Marine Geology, 58(3-4), 345-371.

Meng, X., Chen, Y., Wang, B., Ma, Q. W., & Wang, F. J. (2016). Responses of phytoplankton community to the input of different aerosols in the East China Sea. Geophysical Research Letters, 43(13), 7081-7088.

Moore, C. M., Mills, M. M., Langlois, R., Milne, A., Achterberg, E. P., La Roche, J., & Geider, R. J. (2008). Relative influence of nitrogen and phosphorous availability on phytoplankton physiology and productivity in the oligotrophic sub-tropical North Atlantic Ocean. Limnology and Oceanography, 53(1), 291-305.

Moore, C. M., Mills, M. M., Arrigo, K. R., Berman-Frank, I., Bopp, L., Boyd, P. W., ... & Ulloa, O. (2013). Processes and patterns of oceanic nutrient limitation. Nature geoscience, 6(9), 701-710.

Moreno, T., Querol, X., Castillo, S., Alastuey, A., Cuevas, E., Herrmann, L., ... & Gibbons, W. (2006). Geochemical variations in aeolian mineral particles from the Sahara–Sahel Dust Corridor. Chemosphere, 65(2), 261-270.

Mounkaila, M. (2006). Spectral and mineralogical properties of potential dust sources on a transect from the Bodélé Depression (Central Sahara) to the Lake Chad in the Sahel. Hohenheimer Bodenkundliche Hefte 78, 1–311.

Nicholson, S. E. (2000). The nature of rainfall variability over Africa on time scales of decades to millenia. Global and planetary change, 26(1-3), 137-158.

Nicholson, S. E. (2013). The West African Sahel: A review of recent studies on the rainfall regime and its interannual variability. International Scholarly Research Notices, 2013.

Otto, S., de Reus, M., Trautmann, T., Thomas, A., Wendisch, M., & Borrmann, S. (2007). Atmospheric radiative effects of an in situ measured Saharan dust plume and the role of large particles. Atmospheric Chemistry and Physics, 7(18), 4887-4903.

Pabortsava, K., Lampitt, R. S., Benson, J., Crowe, C., McLachlan, R., Le Moigne, F. A., ... & Woodward, E. M. S. (2017). Carbon sequestration in the deep Atlantic enhanced by Saharan dust. Nature Geoscience, 10(3), 189-194.

Palchan, D., & Torfstein, A. (2019). A drop in Sahara dust fluxes records the northern limits of the African Humid Period. Nature Communications, 10(1), 3803.

Pausata, F. S., Gaetani, M., Messori, G., Berg, A., de Souza, D. M., Sage, R. F., & DeMenocal, P. B. (2020). The greening of the Sahara: Past changes and future implications. One Earth, 2(3), 235-250.

Piperno, D. R. (2001). Phytoliths. Tracking Environmental Change Using Lake Sediments: Terrestrial, Algal, and Siliceous Indicators, 235-251.

Pokras, E. M., & Mix, A. C. (1985). Eolian Evidence for Spatial Variability of Late Quaternary Climates in Tropical Africa1. Quaternary Research, 24(2), 137-149.

Prospero, J. M., Olmez, I., & Ames, M. (2001). Al and Fe in PM 2.5 and PM 10 suspended particles in south-central Florida: The impact of the long range transport of African mineral dust. Water, Air, and Soil Pollution, 125, 291-317.

Prospero, J. M., Ginoux, P., Torres, O., Nicholson, S. E., & Gill, T. E. (2002). Environmental characterization of global sources of atmospheric soil dust identified with the Nimbus 7 Total Ozone Mapping Spectrometer (TOMS) absorbing aerosol product. Reviews of geophysics, 40(1), 2-1.

Prospero, J. M., & Lamb, P. J. (2003). African droughts and dust transport to the Caribbean: Climate change implications. Science, 302(5647), 1024-1027.

Pye, K. (1987). Aeolian Dust and Dust Deposits. Elsevier, 334 pp.

Pye, K. (1989). Processes of fine particle formation, dust source regions, and climatic changes. In Paleoclimatology and Paleometeorology: Modern and Past Patterns of Global Atmospheric Transport (pp. 3-30). Dordrecht: Springer Netherlands.

Reid, J. S., Reid, E. A., Walker, A., Piketh, S., Cliff, S., Al Mandoos, A., ... & Eck, T. F. (2008). Dynamics of southwest Asian dust particle size characteristics with implications for global dust research. Journal of Geophysical Research: Atmospheres, 113(D14).

Reille, M. (1999). Pollen et spores d'Europe et d'Afrique du Nord. FeniXX.

Richter, T. O., Van der Gaast, S., Koster, B., Vaars, A., Gieles, R., de Stigter, H. C., ... & van Weering, T. C. (2006). The Avaatech XRF Core Scanner: technical description and applications to NE Atlantic sediments. Geological Society, London, Special Publications, 267(1), 39-50.

Ridame, C., & Guieu, C. (2002). Saharan input of phosphate to the oligotrophic water of the open western Mediterranean Sea. Limnology and Oceanography, 47(3), 856-869.

Rodríguez, S., Alastuey, A., Alonso-Pérez, S., Querol, X., Cuevas, E., Abreu-Afonso, J., ... & De la Rosa, J. (2011). Transport of desert dust mixed with North African industrial pollutants in the subtropical Saharan Air Layer. Atmospheric Chemistry and Physics, 11(13), 6663-6685.

Rolph, G., Stein, A., and Stunder, B., (2017). Real-time Environmental Applications and Display sYstem: READY. Environmental Modelling & Software, 95, 210-228, https://doi.org/10.1016/j.envsoft.2017.06.025

Romero, O. E., Dupont, L., Wyputta, U., Jahns, S., & Wefer, G. (2003). Temporal variability of fluxes of eolian-transported freshwater diatoms, phytoliths, and pollen grains off Cape Blanc as reflection of land-atmosphere-ocean interactions in northwest Africa. Journal of Geophysical Research: Oceans, 108(C5).

Schepanski, K., Tegen, I., Laurent, B., Heinold, B., & Macke, A. (2007). A new Saharan dust source activation frequency map derived from MSG-SEVIRI IR-channels. Geophysical Research Letters, 34(18), L18803.

Schepanski, K., Tegen, I., Todd, M. C., Heinold, B., Bönisch, G., Laurent, B., & Macke, A. (2009). Meteorological processes forcing Saharan dust emission inferred from MSG-SEVIRI observations of subdaily dust source activation and numerical models. Journal of geophysical research: atmospheres, 114(D10).

Schepanski, K., Tegen, I., & Macke, A. (2012). Comparison of satellite based observations of Saharan dust source areas. Remote Sensing of Environment, 123, 90-97.

Scheuvens, D., Schütz, L., Kandler, K., Ebert, M., & Weinbruch, S. (2013). Bulk composition of northern African dust and its source sediments—A compilation. Earth-Science Reviews, 116, 170-194.

Schuster, M., Roquin, C., Duringer, P., Brunet, M., Caugy, M., Fontugne, M., ... & Ghienne, J. F. (2005). Holocene lake Mega-Chad palaeoshorelines from space. Quaternary Science Reviews, 24(16-17), 1821-1827.

Servant, M. (1983). Séquences continentales et variations climatiques: évolution du bassin du Tchad au Cénozoïque supérieur. FeniXX.

Simpson, D. A., Yesson, C., Culham, A., Couch, C. A., & Muasya, A. M. (2011). Climate change and Cyperaceae. Climate change, ecology and systematics, 439-456.

Spaulding, S. A., Potapova, M. G., Bishop, I. W., Lee, S. S., Gasperak, T. S., Jovanoska, E., ... & Edlund, M. B. (2021). Diatoms.org: supporting taxonomists, connecting communities. Diatom Research, 36(4), 291-304.

Stein, A.F., Draxler, R.R, Rolph, G.D., Stunder, B.J.B., Cohen, M.D., and Ngan, F., (2015). NOAA's HYSPLIT atmospheric transport and dispersion modeling system, Bull. Amer. Meteor. Soc., 96, 2059-2077, http://dx.doi.org/10.1175/BAMS-D-14-00110.1

Stuut, J. B. W., Prins, M. A., Schneider, R. R., Weltje, G. J., Jansen, J. F., & Postma, G. (2002). A 300-kyr record of aridity and wind strength in southwestern Africa: inferences from grain-size distributions of sediments on Walvis Ridge, SE Atlantic. Marine Geology, 180(1-4), 221-233.

Stuut, J. B., Zabel, M., Ratmeyer, V., Helmke, P., Schefuß, E., Lavik, G., & Schneider, R. (2005). Provenance of present-day eolian dust collected off NW Africa. Journal of Geophysical Research: Atmospheres, 110(D4).

Stuut, J. B., Smalley, I., & O'Hara-Dhand, K. (2009). Aeolian dust in Europe: African sources and European deposits. Quaternary International, 198(1-2), 234-245.

Talbot, R. W., Harriss, R. C., Browell, E. V., Gregory, G. L., Sebacher, D. I., & Beck, S. M. (1986). Distribution and geochemistry of aerosols in the tropical North Atlantic troposphere: Relationship to Saharan dust. Journal of Geophysical Research: Atmospheres, 91(D4), 5173-5182.

Talling, J. F. (1980). Some problems of aquatic environments in Egypt from a general viewpoint of Nile ecology. Water Supply and Management, 4(1-2).

Taylor, J. C., Cocquyt, C., & Mayama, S. (2016). New and interesting Eunotia (Bacillariophya) taxa from the Democratic Republic of the Congo, tropical central Africa. Plant Ecology and Evolution, 149(3), 291-307.

Tiedemann, R., Sarnthein, M., & Shackleton, N. J. (1994). Astronomic timescale for the Pliocene Atlantic δ18O and dust flux records of Ocean Drilling Program Site 659. Paleoceanography, 9(4), 619-638.

Tsamalis, C., Chédin, A., Pelon, J., & Capelle, V. (2013). The seasonal vertical distribution of the Saharan Air Layer and its modulation by the wind. Atmospheric Chemistry and Physics, 13(22), 11235-11257.

Twohy, C. H., Kreidenweis, S. M., Eidhammer, T., Browell, E. V., Heymsfield, A. J., Bansemer, A. R., ... & Van Den Heever, S. C. (2009). Saharan dust particles nucleate droplets in eastern Atlantic clouds. Geophysical Research Letters, 36(1).

Van Der Does, M., Korte, L. F., Munday, C. I., Brummer, G. J. A., & Stuut, J. B. W. (2016). Particle size traces modern Saharan dust transport and deposition across the equatorial North Atlantic. Atmospheric Chemistry and Physics, 16(21), 13697-13710.

Van Der Does, M., Knippertz, P., Zschenderlein, P., Giles Harrison, R., & Stuut, J. B. W. (2018). The mysterious long-range transport of giant mineral dust particles. Science advances, 4(12), eaau2768.

Van der Does, M., Brummer, G.-J. A., Van Crimpen, F. C. J., Korte, L. F., Mahowald, N. M., Merkel, U., et al. (2020). Tropical rains controlling deposition of saharan dust across the north atlantic ocean. Geophysical Research Letters, 47, e2019GL086867. https://doi.org/10.1029/2019GL086867

Van der Does, M., Brummer, G. J. A., Korte, L. F., & Stuut, J. B. W. (2021). Seasonality in Saharan dust across the Atlantic Ocean: From atmospheric transport to seafloor deposition. Journal of Geophysical Research: Atmospheres, 126(11), e2021JD034614.

Van der Jagt, H., Friese, C., Stuut, J. B. W., Fischer, G., & Iversen, M. H. (2018). The ballasting effect of Saharan dust deposition on aggregate dynamics and carbon export: Aggregation, settling, and scavenging potential of marine snow. Limnology and Oceanography, 63(3), 1386-1394.

Washington, R., Todd, M. C., Lizcano, G., Tegen, I., Flamant, C., Koren, I., ... & Prospero, J. M. (2006). Links between topography, wind, deflation, lakes and dust: The case of the Bodélé Depression, Chad. Geophysical research letters, 33(9).

Weltje, G.J., Prins, M.A. (2003). Muddled or mixed? Inferring palaeoclimate from size distributions of deep-sea clastics. Sedimentary Geology 162 (1), 39–62

Weltje, G. J., & Tjallingii, R. (2008). Calibration of XRF core scanners for quantitative geochemical logging of sediment cores: Theory and application. Earth and Planetary Science Letters, 274(3-4), 423-438.

White, F. (I983). The vegetation of Africa. Natural Resources Research, UNESCO, Vol. 20, 356 pp.

Yu, H., Chin, M., Bian, H., Yuan, T., Prospero, J. M., Omar, A. H., ... & Zhang, Z. (2015). Quantification of trans-Atlantic dust transport from seven-year (2007–2013) record of CALIPSO lidar measurements. Remote Sensing of Environment, 159, 232-249.

Zarasvandi, A. (2009). Environmental impacts of dust storms in the Khuzestan province. Environmental Protection Agency (EPA) of Khuzestan province, Internal Report, 375p.

Ziman, S. N., & Keener, C. S. (1989). A geographical analysis of the family Ranunculaceae. Annals of the Missouri Botanical Garden, 1012-1049.

Supplementary materials

Sample number	**Date**	**Position** (Lat N)	**Position** (Long E)	**Filtered volume** (L)	**Water temperature** (°C)
W1	13/12/2023	27°53.336	−15°16.860	59.1	21.8
W2	14/12/2023	25°12.188	−17°55.632	38.6	22.9
W3	15/12/2023	22°35.714	−21°43.585	40	24.0
W4	16/12/2023	20°27.385	−24°42.751	41.1	25.0
W5	17/12/2023	18°46.217	−27°49.520	40	25.0
W6	18/12/2023	17°50.484	−31°27.144	40	25.5
W7	19/12/2023	17°15.765	−35°13.471	40	26.0
W8	20/12/2023	15°50.863	−38°58.761	40	26.5
W9	21/12/2023	15°14.609	−42°13.757	40	27.0
W10	22/12/2023	14°35.370	−45°13.668	40	27.2
W11	23/12/2023	13°34.522	−47°41.489	40	27.5
W12	24/12/2023	12°45.602	−50°07.643	40	27.5
W13	25/12/2023	12°18.965	−52°12.856	40	28.2
W14	26/12/2023	12°24.495	−53°51.313	40	29.0
W15	27/12/2023	13°09.419	56°52.986	40	28.2
W16	28/12/2023	14°10.497	60°06.004	40	28.2

Table S1: *Overview of sampling locations and properties of the obtained water samples.*

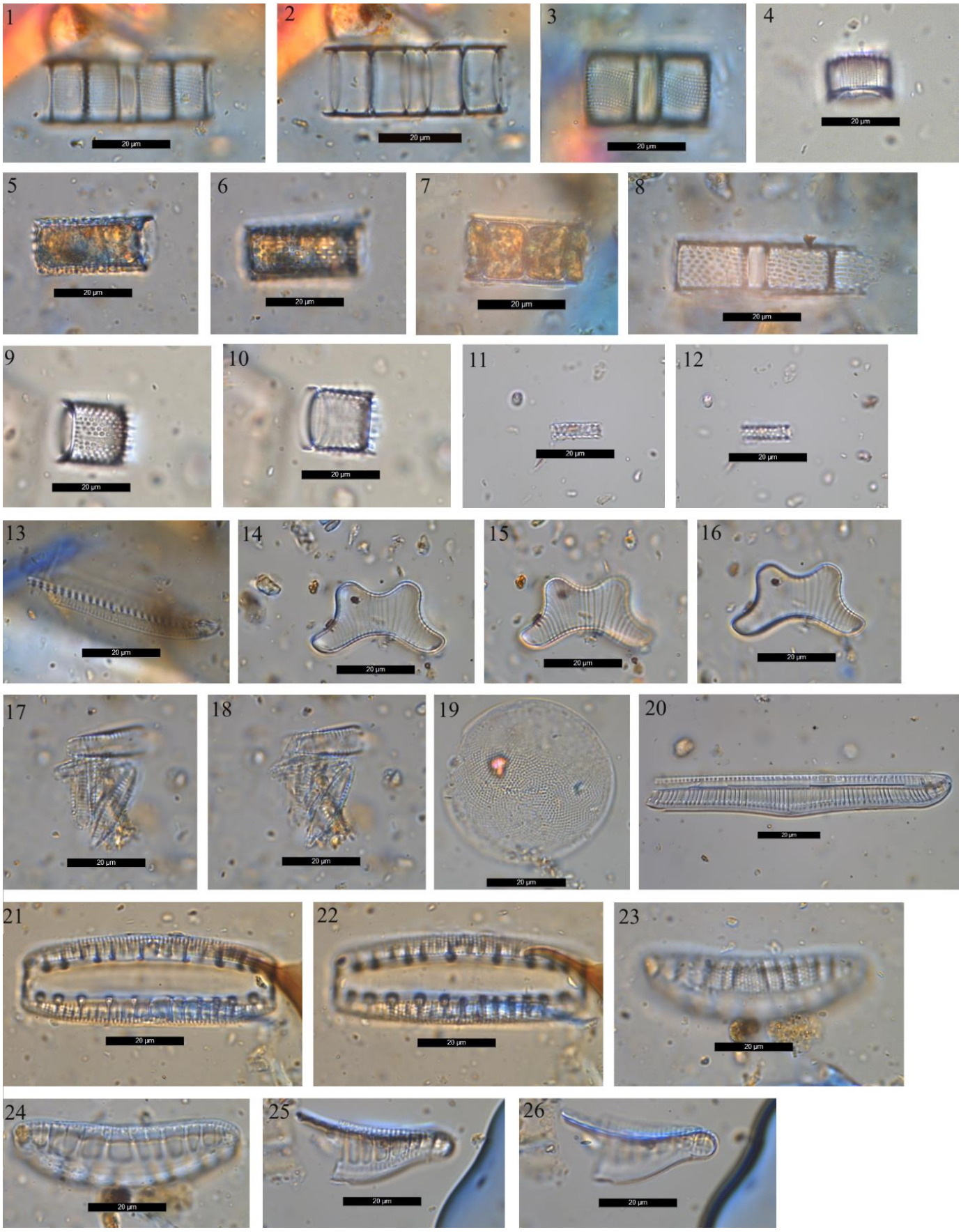

Plate S-1*: LM images of selected algae as examples for identified taxa from dust samples:* ***(1-4)****: Aulacoseira ambigua;* ***(5-7)*** *Aulacoseira containing cellular content;* ***(8-10)****: Aulacoseira granulata;* ***(11-12)****: Aulacoseira granulate var. angustissima;* ***(13)****: Nitzschia;* ***(14-16)****: Eunotia pierrefuseyi;* ***(17-18)****: Fragilaria;* ***(19)****: Melosira;* ***(20)****: Epithemia* cf. *gibba;* ***(21-26)****: Epithemia spp.*

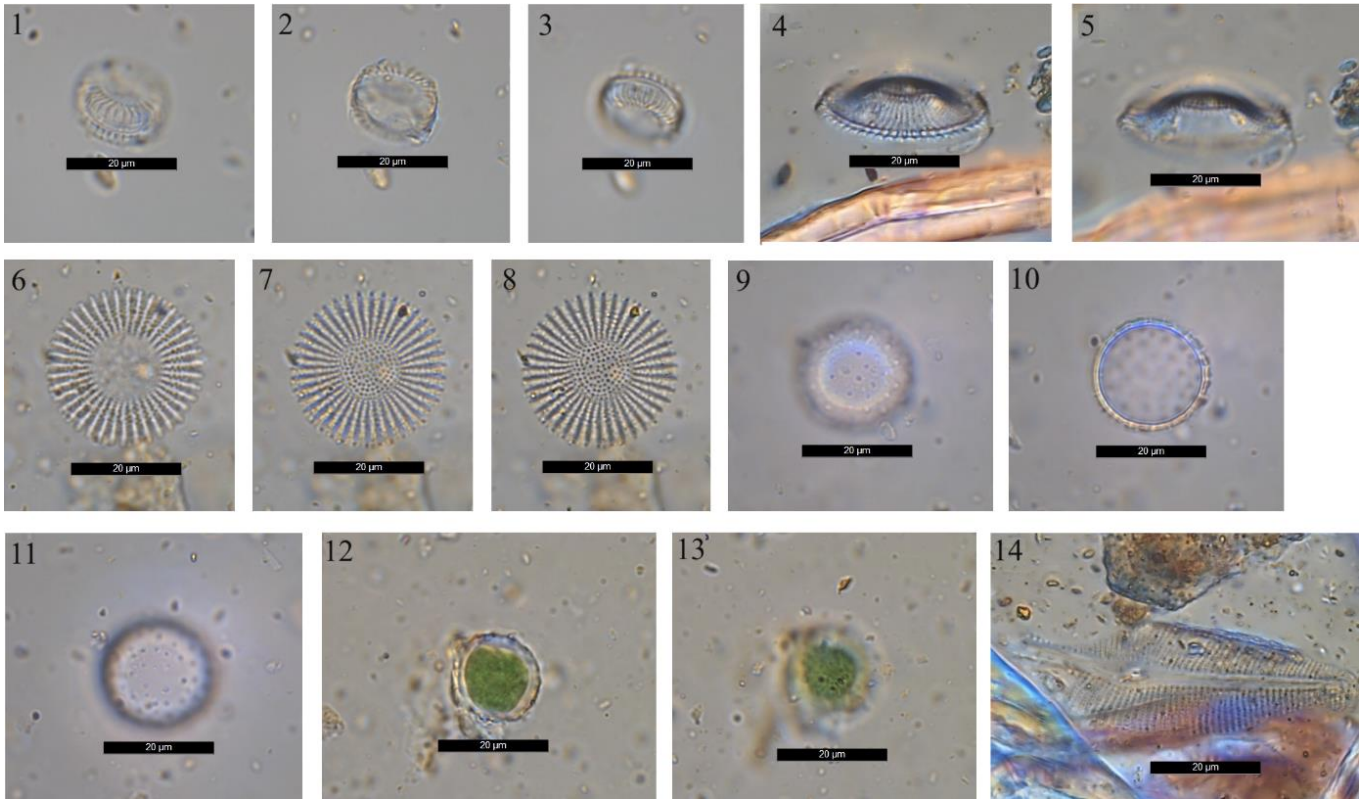

***Plate S-II**: LM images of selected algae as examples for identified taxa from dust samples: (**1-3**): Cyclotella; (**4-8**): Stephanodiscus; (**9-13**): cf. Phacotus; (**14**): Large unidentified diatom 1.*

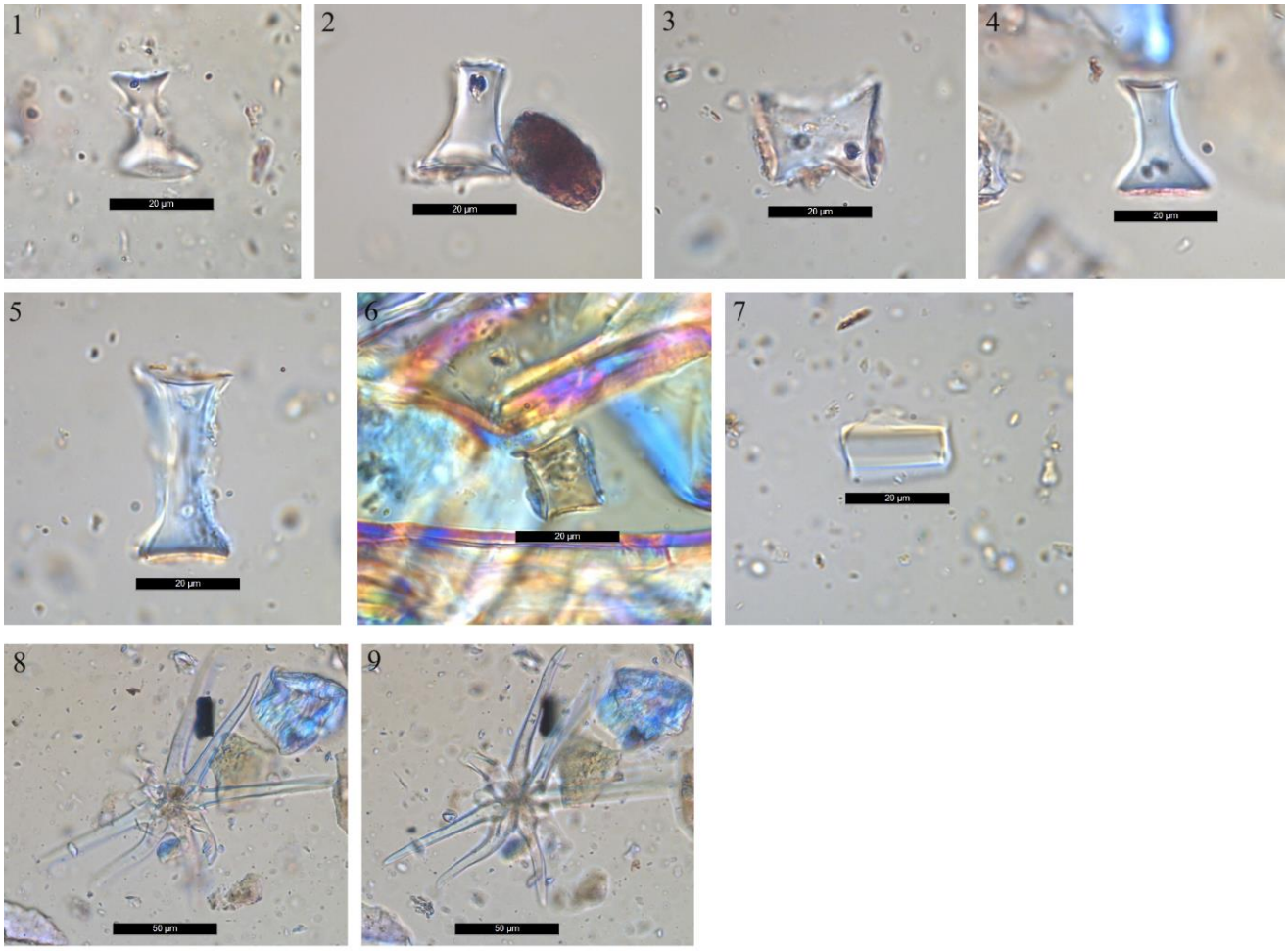

***Plate S-III**: LM images of the trichome and phytoliths from the dust samples: (**1-7**): Phytoliths; (**8-9**): Trichome.*

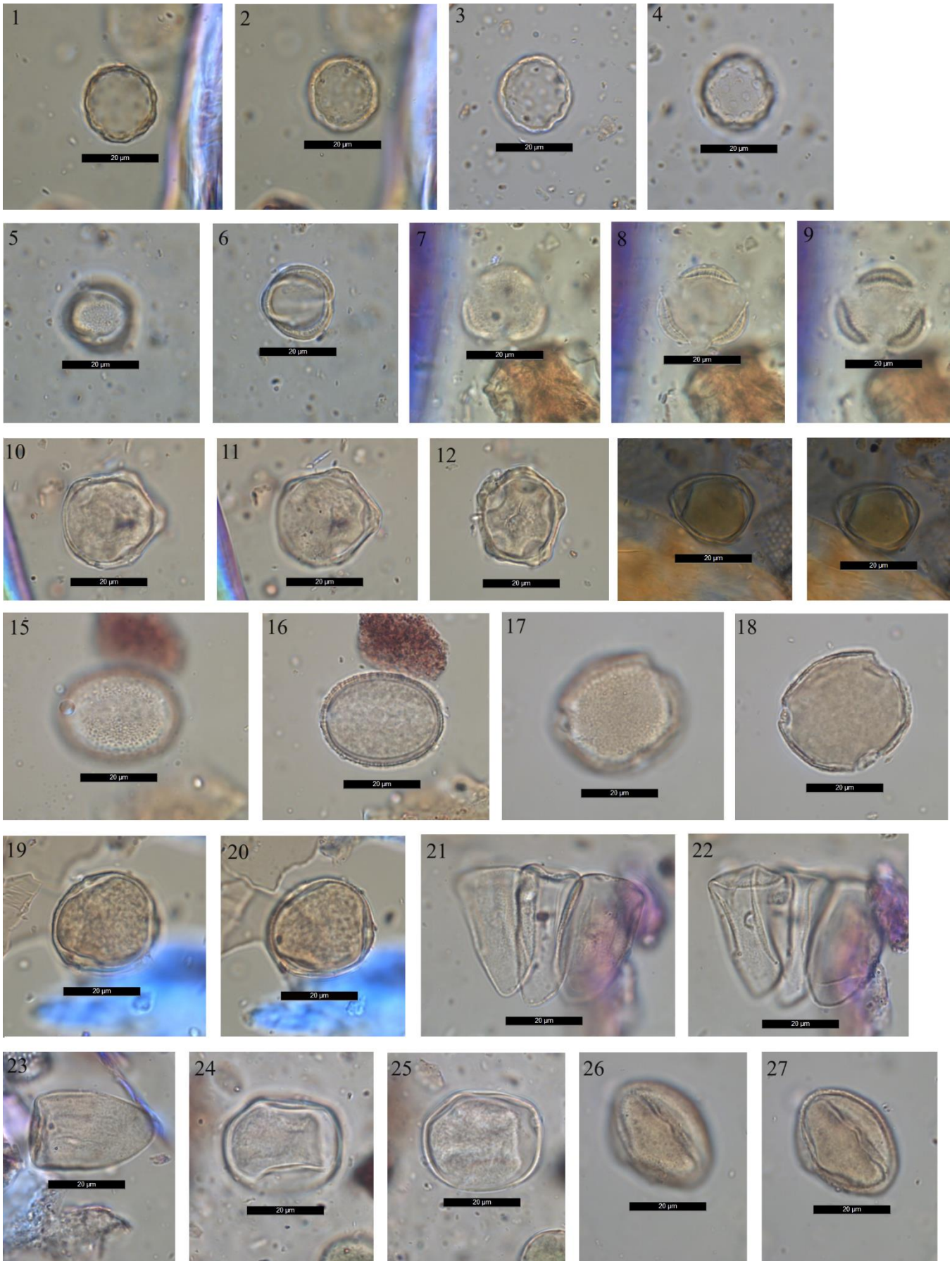

***Plate S-IV**: LM images of selected pollen as examples for identified taxa from dust samples: **(1-4)**: Amaranthaceae-Chenopodiaceae spp.; **(5-9)**: Artemisia; **(10-12)**: Alnus; **(13-14)**: Corylus; **(15-16)**:* cf. *Neslia; **(17-18)**: Campanula; **(19-20)**: Cannabis; **(21-25)**: Cyperaceae spp.; **(26-27)**: Ephedra.*

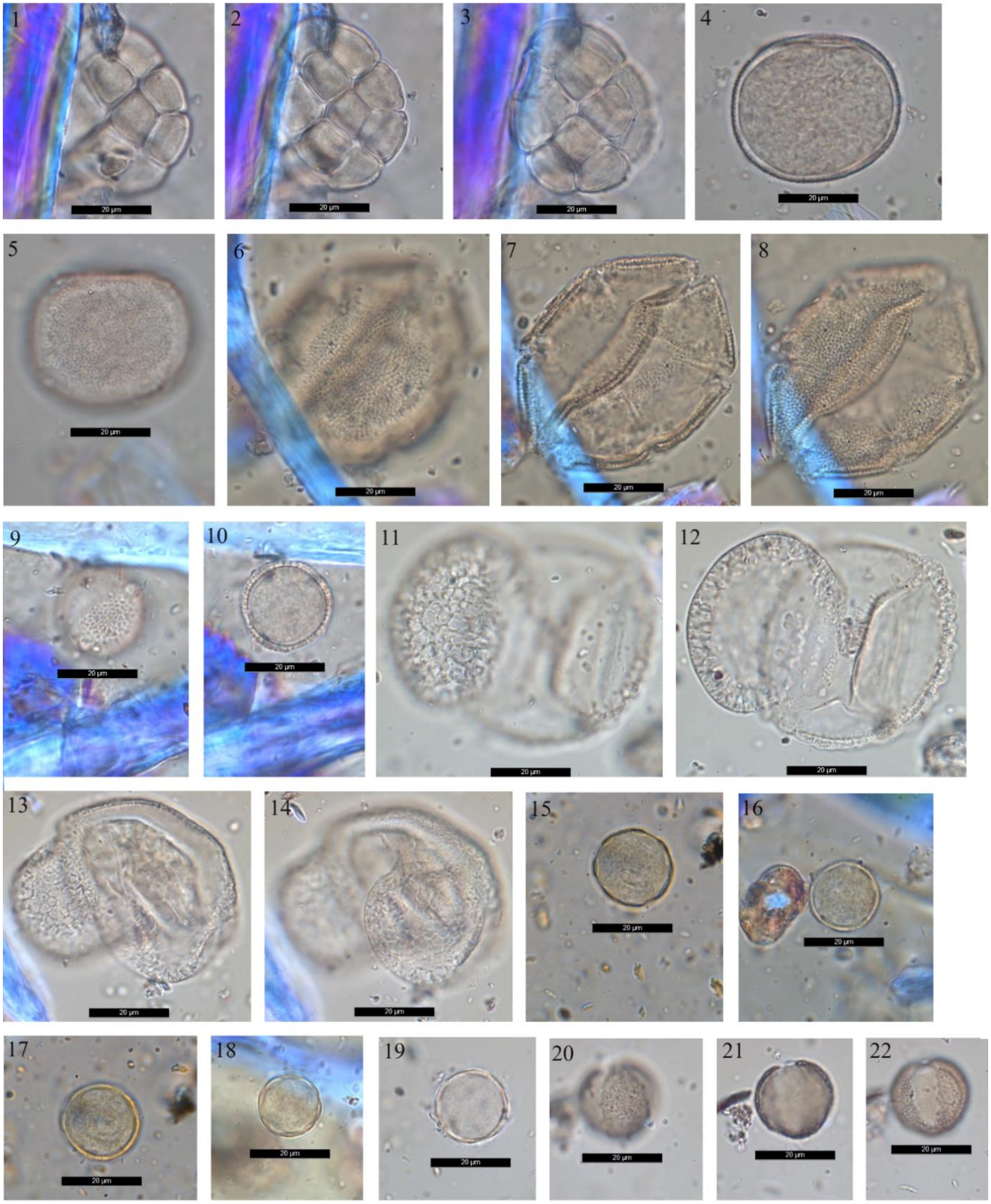

Plate S-V*: LM images of selected pollen as examples for identified taxa from dust samples: (**1-3**): Acacia; (**4-5**): Ornithogalum; (**6-8**): Lamiaceae Sp.; (**9-10**): Ligustrum; (**11-14**): Pinus* spp.*; (**15-19**): Thalictrum; (**20-22**): Ranunculaceae.*

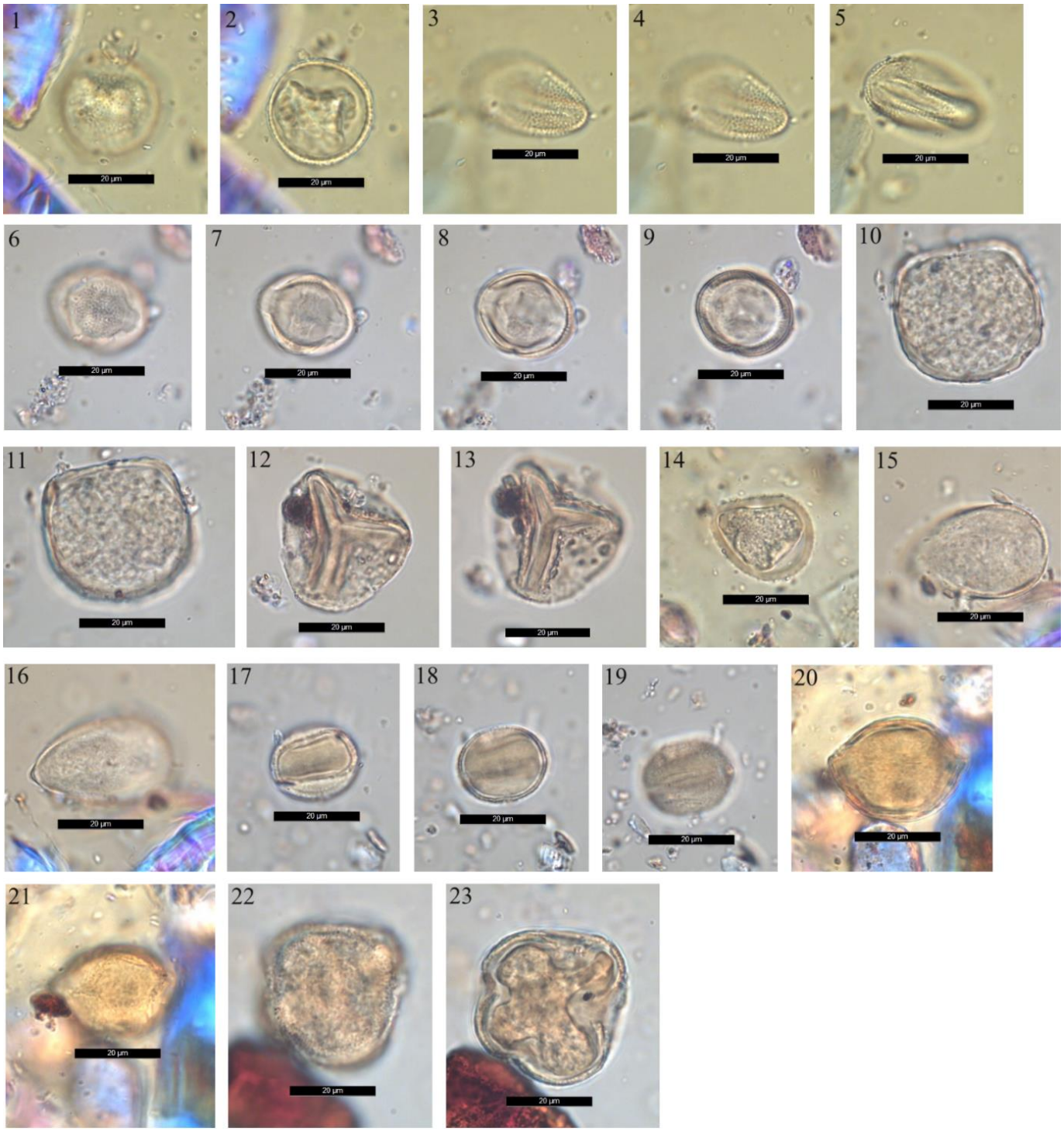

***Plate S-VI**: LM images of selected pollen as examples for identified taxa from dust samples: (**1-2**): Populus; (**3-5**): Saxifraga; (**6-9**): Verbascum; (**10-11**): Ulmus; (**12-13**): Trilete spore; (**14**): Unidentified pollen taxa 1; (**15-16**): Unidentified pollen taxa 2; (**17-19**): Unidentified pollen taxa 3; (**20-21**): Unidentified pollen taxa 4; (**22-23**): Unidentified pollen taxa 5.*

Element / Sample	Mg	Al	Si	P	S	Cl	K	Ca	Ti	V	Mn	Fe	Ba
A1	1113.4	23928.4	148695.4	783.4	3972.8	12446	51878.6	83648	24160	2692	3552.8	241029.2	2083
A2	1124.6	19147.4	117180.6	974.2	5530.6	11429.4	43357.4	49058.6	17318.6	2874.8	2966.4	196754	2191.4
A3	973.2	20855.8	128416	882.6	5275.2	11294.2	43325.2	48266	24076.8	3112.2	3579.8	253190.6	2339.8
A4	1407.6	35117.4	216338.2	1161.8	5864	15804	68117.4	74379	28993.6	2837.6	4482	272428.2	2520.4
A5	2225.8	45608.8	280292	1492.6	6258	29672.8	112703.4	144807.6	47809.8	2869.8	7854.2	478994	2946
A6	1318	30743.6	183292.6	900.4	3679.4	12470.6	64264	51338.4	27977.2	2960.2	4460.8	267901.2	2469.6
A7	1297	25697.6	157501.6	713	4356	11841.8	57741.8	69260.4	24217	2782.2	4326.4	247259	2642.4
A8	1098.6	21758.8	130574	851.6	4903	12903.4	51592.6	57015.4	20641.6	3059	3891	236471	2420.6
A9	1236.4	27731.4	164223.8	946	4268.2	10651	59229.4	46946.6	21201.4	2807	3685.6	227559.8	2506.4
A10	1402.8	30817.8	180118	1137	5649.8	14478.2	69534.6	48258.8	26064.4	2875.6	4941.2	298196.4	2668.4
A11	697.6	9033	58331.8	171	3208	14153	13482.6	17924	5541.8	3025.6		58643	2329.6
A12	589	6305.4	39970.8	124	2432	6623	7231.2	14826.2	4352.4	2724.6		11683.4	1643.2
A13	529.4	5657.4	37571.2	538	2748.4	9178.2	7894.2	19242	1932.4	2346.4		13652.2	1589
A14	719.4	9573.2	61604.4	642.4	3133.2	13697	17393.4	22070	4664.6	2846.2		63498.8	1580.8
A15	556.8	5345.8	36040	130.6	3423.4	15786.2	13029.2	21065.6	7531.8	2577.6		56975	2446.6

Table S2: *Bulk chemical composition of atmospheric dust samples, measured using XRF-analysis at 10 Kv and expressed in absolute counts.*

Element / Sample	Mn	Fe	Co	Ni	Cu	Zn	Br	Rb	Sr	Y	Zr	Rh ch.	Rh inch.	Pb	U
A1	867.8	90874.4	820.8	5358.6	1577	3009.6	958.8	1450.8	2939.4	1713	2299.8	18109.4	126412.2	1320.6	1340.6
A2	631	66421.8	538.4	5227.2	1554.8	23780	911.4	1412.6	2313.2	1227.6	1714	18110.8	129083.2	1301.8	1289.4
A3	711	84020	724.2	4811.2	1539.4	22032.4	913	1470.2	2796.8	1242.5	2153	17566	125782.6	1296.8	1210.2
A4	992.6	95685.6	764	4985.6	1529.8	23650.8	868.2	1586.8	2991.8	1110.8	2243	18081.6	125128.8	1257.6	1187.2
A5	1667.8	169228.8	2946	1503.4	4244.8	990.2	1841.4	2432	4895.8	1367.2	3392.8	17715	101283.4	1020	895.4
A6	947.8	92497.2	831.8	4745.2	1377.2	2655	825.2	1510.2	2820.6	1567	1959	18260.4	127755.6	1271	1435.2
A7	971.8	92920.6	848.4	4740.2	1263.6	1857.8	830.6	1633.2	2991.2	1647.4	2054.2	17901.4	127526	1383.6	1301.8
A8	909.2	84705.8	695.4	4741.2	1048.8	22383.6	995.6	1559.6	3272.8	1410.8	2039.2	18042.4	128252	1190.6	1451.4
A9	815.4	77172.6	649	4894.6	1027.6	22948.4	880.8	1382.4	2875.6	1285	1968.4	18167.8	128978.4	1297.6	1418.8
A10	1069.6	102729	871	4732.6	1149.8	21813.4	844.2	1752.6	3235	1502.25	2056.4	18072.6	125451	1300	1292.8
A11	172.2	18074.8	173.4	5022.4	983	457.8	1128.6	1058.8	2140.6	1328.2	1345.6	17417.8	133503.6	1414.6	1549.8
A12		3655.6		5048.2	925	385.2	1111.2	1059.6	1714.2		1020	16632.2	134283.4	1705.4	1599.8
A13	195.2	3598.4		5010.4	881.8	24029	1061.8	1342.6	2161.4	1247.8	1392.6	18017.4	134224.4	1810.2	1578.4
A14	171.2	15465.4		5067	989.8	23912.8	1163	1311	2111.4	1072	1334.4	17640	133648.6	1793.6	1433.8
A15	141.4	16302.8		5073	1143.6	677	1074.4	1050.75	1912.8	1196	1396.4	17436.6	133871.4	1277.4	1499.2

Table S3: *Bulk chemical composition of atmospheric dust samples, measured using XRF-analysis at 30 Kv and expressed in absolute counts.*